**Thesis for Ph. D. degree**

# Low-enthalpy geothermal resource evaluation through simulations of optimal geothermal heat pump systems

# 지열히트펌프시스템의 최적 설계를 통한 저온지열자원의 활용성 평가

**Kim, Seong-Kyun**

**February 2015**

**School of Earth and Environmental Sciences**

**Seoul National University**

# Low-enthalpy geothermal resource evaluation through simulations of optimal geothermal heat pump systems

# 지열히트펌프시스템의 최적 설계를 통한 저온지열자원의 활용성 평가

지도교수 **이 강 근**

이 논문을 이학박사 학위논문으로 제출함
2014년 10월

서울대학교 대학원
지구환경과학부
**김 성 균**

김성균의 이학박사 학위논문을 인준함
2014년 12월

위 원 장 _____ (인)

부위원장 _____ (인)

위 원 _____ (인)

위 원 _____ (인)

위 원 _____ (인)

# Low-enthalpy geothermal resource evaluation through simulations of optimal geothermal heat pump systems

**Kim, Seong-Kyun**

A dissertation submitted in partial fulfillment of

the requirements for the degree of

Doctor of Philosophy

**October 2014**

**School of Earth and Environmental Sciences**

**Seoul National University**

# Abstract

Simulation models for evaluating utilization of low-enthalpy geothermal resources through the optimally designed geothermal heat pump (GHP) system is suggested. Firstly, a numerical model for the simulation of temperature changes in a borehole heat exchanger (BHE) with fluid circulating through U-tubes is developed. The model can calculate the thermal energy transferred from heat pumps to BHEs while considering the nonlinear relationship between temperature of the circulating fluid and the thermal energy. The use of the developed model enables also the design of a GHP system with the view of pursuing efficiency and financial benefit. The developed model is validated by comparing two measurement datasets with their respective simulation results. In addition, it is used to analyze the sensitivities of design parameters that can affect the performance of the closed-loop GHP system. The most sensitive parameters on the system are the thermal conductivity of the ground and the Darcian groundwater velocity considering acceptable distribution range in the realm of nature. Maximum change of the circulating fluid temperature at the BHE outlet is about 4℃ when thermal conductivity of the ground changes from 2 W/mK to 5 W/mK and the Darcian groundwater velocity changes from $10^{-8}$ m/s to $10^{-6}$ m/s, respectively. The numerical evaluation of a real GHP system with 28 BHEs and 79 heat pumps involves consideration of the base case and modified cases. In all cases, the temperatures of the circulating fluid at the BHE inlet and outlet,

heat pump efficiency, and the heating power and electric power of heat pumps are obtained. The most cost-effective system in this case is for there to be 4, 6, and 6 BHEs on the first, second, and third floors, respectively.

The next version of the numerical simulator and grid generator is developed to consider multiple BHEs simultaneously. Thus, massively parallel computing procedures into the simulator are introduced to improve distributing memory requirements and computational efficiency for solving large simulation problems with a great number of grid-blocks. The new grid generator is designed to produce a simulation domain with multiple BHEs. The newly developed simulation model can consider thermal interactions among BHEs when the system is in operation and storing thermal energy in the ground after the operation period of the system. These two mechanisms should be considered in the evaluation of long-term performance of the BHE. The developed simulation model is tested for the performance improvement through parallelization. The computational efficiency of the developed simulation model is considerably increased in direct proportion to the number of the processors. The model is then applied to evaluate the performance of the KIGAM GHP system for a 25-year operation. The temperature of the ground in the vicinity of BHEs is gradually increased with time because of the imbalance of the injected/extracted thermal power to/from the ground during the cooling/heating seasons. It causes the decrease of the efficiency of the system during the cooling seasons for the long-term operation.

Finally, a versatile simulation model is developed to simulate not only the vertical closed-loop GHP system, but also the standing column well and open-loop GHP systems. A method to generate an unstructured Voronoi grid for its use in simulations of geothermal heat pump systems is presented. A series of codes is developed to create Voronoi cell center points that are placed at specific positions for well- or pipe-shaped Voronoi grids, to generate a three-dimensional grid from generated Voronoi cell vertices, and to visualize the generated grid and simulation results by ParaView. AMESH program is used to calculate the x- and y-coordinates of the Voronoi cell vertices from the Voronoi cell center points. The developed series of codes can generate the desired form of the grid. The generated grid is tested with confidence through simulations of water production/injection from/to the various kinds of the geothermal wells.

**Keywords:** geothermal heat pump, borehole heat exchanger, design optimization, long-term performance, TOUGH2, integral finite difference method

**Student number:** 2004-20564

# Contents

# List of Tables

# List of Figures

# Chapter 1. Introduction

## 1.1. Backgrounds

Geothermal energy, one of the new and renewable energy, has until recently had little economic potential except in areas where high-enthalpy geothermal energy resources, i.e. thermal water or steam, are found. This has lately changed with developments of geothermal heat pump (GHP) systems, sometimes referred to as ground-source heat pump (GSHP) systems, using low-enthalpy geothermal energy resources for heating and cooling purposes (Fridleifsson, 2001). They use the almost constant temperature of the shallow ground as the exchange medium instead of the outside air temperature. This allows that the electrical efficiency of the GHP system is better than that of the air-source heat pump (ASHP) system because ground temperature is higher than air temperature in the heating season and is lower than air temperature in the cooling season. Now the GHP systems have been popular in many countries regardless of weather conditions, including South Korea.

There are three basic types of GHP systems:

(1) closed-loop systems;

(2) open-loop systems;

(3) standing column well systems.

The closed-loop GHPs circulate a mixture of water and antifreeze through a closed

loop that is buried underground. The loop tubing can be installed horizontally as a loop field in trenches or vertically as a series of long U-shapes in boreholes. The open-loop GHP system produces groundwater directly from wells. Once the produced groundwater has circulated through the system, it returns back to the ground through injection wells or is discharged into the surface. The standing column well (SCW) system is a specialized type of open loop system. Groundwater is produced from the bottom of a deep well, passed through a heat pump, and injected back to the top of the well, where flowing downwards it exchanges heat with the geologic medium or groundwater. The schematics of these systems are shown in Figure 1.1.

All GHP systems tend to have higher initial costs than ASHP systems or conventional heating, ventilating and air conditioning (HVAC) systems, due to the expense of drilling wells, installing pipes, and so on. The vertical closed-loop GHP system, which is the most popular GHP system (Lund et al., 2004), typically has the highest initial costs of the other GHP systems. It requires more number of wells, called borehole heat exchangers (BHEs), than the others because of the lower efficiency. Moreover, the BHE is not just empty well, but equipped with pipes, called a U-tube, and filled with grouting materials surrounding the U-tube. They are major causes of the highest initial costs. The initial cost of the horizontal closed-loop GHP system depends on the price of land because it requires a large area for installing the long trench. The open-loop and SCW systems have a cost problem in the case that the bedrock is so soft that the casing should be needed to prevent the collapse of the

well or the groundwater table is located at deep depths.

In addition, the performance of the GHP system cannot be correctly estimated without knowing the geothermal and hydrogeological properties. However, those properties are typically not measured in most places. The properties related to the conductive/advective heat transport are mainly required for the proper sizing of the closed/open-loop GHP systems. The proper design of the system is necessary to assure long-term performance and to increase energy savings of the system. An over-designed system can increase the initial costs and make the system unattractive financially over the short term. An under-designed system can increase the operational costs that are the greatest benefits of the GHP system and will strain to reach the desired heating and cooling needs. Therefore, the design of the system should be optimized using a quantitative and reliable assessment procedure.

This study is mainly focused on the design of the vertical closed-loop GHP system. The assessment procedure for the design of this system requires an understanding and corresponding treatment of the physical processes in the ground and BHEs, as well as in engineering systems for the heating and cooling of buildings. The heat of indoor air is delivered by a heat pump to circulating fluid in the cooling season. The circulating fluid transports heat through a U-tube mainly by convection, and transports the heat to the ground mainly by conduction. The conducted heat raises the temperature of the ground and groundwater. The opposite process occurs in the heating season. Therefore, the model for designing the system has to be able to consider heat transfer mechanisms in these cyclic processes.

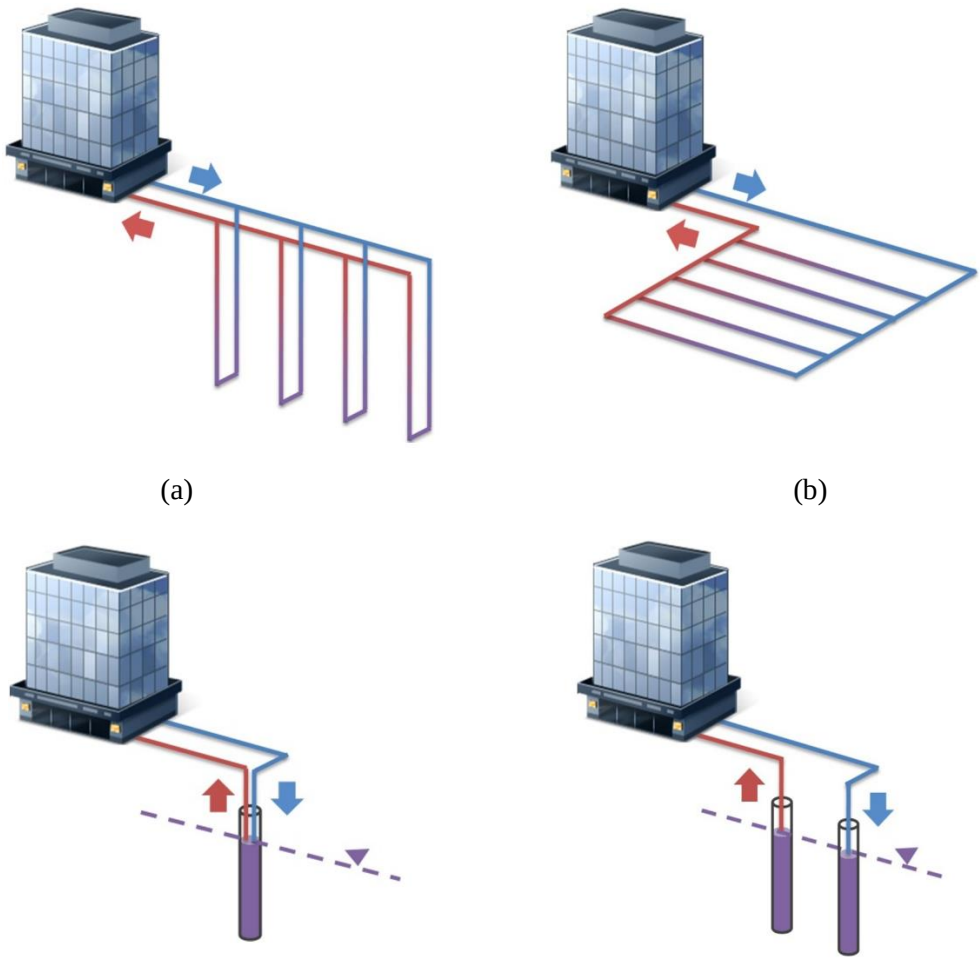


**Figure 1.1.** Types of the geothermal heat pump system: (a) vertical closed-loop, (b) horizontal closed-loop, (c) standing column well, and (d) open-loop. Cold water from heat pumps is injected into the ground and then warm water heated by ground is produced for heating operation.

The earliest approaches for calculating the heat transfer around a BHE used Kelvin's line source model (Ingersoll and Plass, 1948; Ingersoll et al., 1950; Penrod, 1954). Kelvin's line source model assumes the BHE to be an infinite constant-strength line-source within a homogeneous, isotropic, and infinite medium. Kavanaugh and Rafferty (1997) developed a cylindrical source model that considers a single isolated pipe surrounded by an infinite solid with constant properties. The model can be used to calculate the temperatures of the circulating fluid at the BHE inlet and outlet. Analytical models such as the line source model and cylindrical source model have the advantages of simplicity of implementation and high calculation speed in comparison with numerical models. However, they have limitations in terms of the heterogeneous and anisotropic ground and BHE conditions affecting the performance of the BHE.

Numerical models have been developed to overcome limitations of analytical solutions. Using a two-dimensional finite-difference model, Eskilson (1987) developed a solution for the heat flow using functions for the BHE pattern and geometry, called g-functions. The g-functions are related to the spacing between BHEs, and the length and radius of each BHE. Eskilson's solution is not accurate when the term for the heat rejection/extraction is less than 3–6 hours. Yavuzturk et al. (1999) developed a two-dimensional finite-volume model. They used an algebraic algorithm to automatically generate BHE-shaped grids in polar coordinates for the BHE geometry. Gehlin and Hellström's (2003) approach to groundwater flow and its effect in the vicinity of a BHE is based on a two-dimensional finite-difference model.

To demonstrate the influence of topographical and groundwater effects, Signorelli (2004) improved the three-dimensional finite-element model FRACTure (Kohl and Hopkirk, 1995) so that it was suitable for BHE modeling with a fine BHE-shaped grid. However, the fully numerical models have not been applied to the evaluation and optimization of the BHE design. Instead, they were applied to evaluate simpler problems such as thermal response tests for measuring in situ thermal conductivity.

## 1.2. Objectives

The main objective of this study is to evaluate the design and performance of geothermal heat pump systems, especially of vertical closed-loop systems, through simulation modeling of the physical processes in the ground, borehole, and engineering systems such as heat pumps and fluid pumps. The numerical simulator and grid generator are developed to accomplish this objective. They have been gradually upgraded to evaluate the design and performance of the system more realistically and accurately.

The first version of the numerical simulator is developed by modifying TOUGHREACT (Xu et al., 2004). TOUGHREACT is a 3-D numerical simulator that can minimize assumptions and limitations in the simulation model. It can simulate fluid flow according to Darcy's law and heat transport by means of conduction and convection in porous and fractured media. It should be modified to calculate the turbulent heat transfer between the flowing fluid and pipe wall, to

simulate the continuous circulation of the fluid through the pipe, and to calculate the thermal load from the heat pumps. The concepts of the last two modifications are newly introduced in this study, on the contrary, the concept of the first modification is already introduced in the previous research (Signorelli, 2004). The first version of the grid generator is developed to include the shape of the cross-section of the BHE into the TOUGHREACT grid. The shape of the cross-section of the BHE appears a large circle (borehole) containing a couple of small circles (pipes). Only one BHE can be included in this version of the grid generator.

In chapter 2, the first versions of the numerical simulator and grid generator are applied to the sensitivity analysis and the design evaluation. The sensitivity analysis is performed with design parameters that can affect the performance of the BHE. This can be accomplished because the developed model takes these parameters into account. The reliable simulation model that can estimate the power consumption of heat pumps and the operation costs, such as this model, is required for the design evaluation of the GHP system.

The second version of the numerical simulator upgraded from the first version is developed by modifying TOUGH2-MP (Zhang et al., 2008), instead of TOUGHREACT. TOUGH2-MP is a massively parallel version of the TOUGH2 (Pruess et al., 1999) code, so that the computational efficiency and distributing memory requirements of the numerical simulator are improved. The aim of this upgrade is to simulate the vertical closed-loop GHP system that consists of multiple BHEs. Hence, one or more BHEs can be included in the second version of the grid

generator. These upgrades enable the simulation model to consider thermal interactions between BHEs and thermal storage in the ground after the operation period of the system. The modification of TOUGH2-MP is in the same manner as it of TOUGHREACT.

In chapter 3, the second versions of the numerical simulator and grid generator are applied to evaluate the long-term performance of the KIGAM GHP system. The thermal interactions and thermal storage can affect the long-term performance of the GHP system.

The latest version of the numerical simulator upgraded form the second version is also based on TOUGH2-MP. Now, using this numerical simulator, it has become possible to simulate the SCW and open-loop systems. Accordingly, the modification is focused on the modules for processing inputs and outputs of these systems. In the latest version of the grid generator, an adaptive gridding technique, known as Voronoi tessellation, is introduced. It is flexible to include detailed shapes of the cross-sections of pipes at any position inside the geothermal wells, and always satisfies the orthogonal condition of the TOUGH2 grid, which is that connections between two adjacent grid blocks in a TOUGH2 grid should be orthogonal to their connection interface. A series of newly developed or already existing codes are used to create Voronoi seeds that are placed at specific positions for the geothermal wells, to calculate the x- and y-coordinates of the Voronoi vertices from the Voronoi seeds, to generate 3-D grids and TOUGH2 input files from Voronoi vertices, and to visualize the generated grid and simulation results with ParaView.

In chapter 4, the desired form of the grid is generated and an example simulation is performed to demonstrate the use of the generated grid that includes four different kinds of geothermal well systems. The simulation model developed in chapter 4 has not used in applications yet. This remains a subject for further study.

# Chapter 2. Simulation modeling of a borehole heat exchanger and the evaluation of the design of the vertical closed-loop geothermal heat pump system

## 2.1. Introduction

In this chapter, a three-dimensional numerical simulation model is developed for evaluating the design of the vertical closed-loop GHP system that is the most popular GHP system but tends to have the highest initial costs of the various GHP systems. The vertical closed-loop GHP system consists of BHEs, heat pumps, and fluid pumps. In developing an accurate and reliable simulation model for it, followings should be considered: (1) the heat transfer in and around BHEs, (2) the characteristics in terms of operation of heat pumps and fluid pumps. The developed simulation model is composed of a modified version of TOUGHREACT to consider such processes and a three-dimensional grid generator to make the grid closer to the shape of the BHE. It is validated by comparing measurement datasets with simulation results. The model is then applied to the sensitivity analysis on parameters of BHE design and the evaluation of BHE performance.

## 2.2. Method

### 2.2.1. Physical background

The general form of the basic mass and energy balance equations in a porous medium is

$$\frac{d}{dt}\int_{V_n} M\,dV_n = \int_{\Gamma_n} \mathbf{F}\cdot\mathbf{n}\,d\Gamma_n + \int_{V_n} q\,dV_n, \tag{2.1}$$

where $V_n$ is an arbitrary subdomain bounded by the closed surface $\Gamma_n$ and **n** is a normal vector on the surface element $d\Gamma_n$ pointing inward into $V_n$. The quantity $M$ denotes the mass or energy per unit volume. **F** represents the mass or heat flux and $q$ represents sources and sinks (Pruess et al., 1999). The volume $V_n$ should be big enough to be a "representative elementary volume" including many pores and mineral grains, so that the continuum approximation for the porous medium is valid.

The mass accumulation term ($M_M$) is

$$M_M = \phi\rho, \tag{2.2}$$

where $\phi$ denotes porosity and $\rho$ denotes density of fluid.

The heat accumulation term ($M_H$) is

$$M_H = (1-\phi)\rho_R c_R T + \phi\rho u, \tag{2.3}$$

where $\rho_R$ is the rock density, $c_R$ is the specific heat of the rock, $T$ is temperature, and $u$ is the specific internal energy of fluid. Within each subdomain $V_n$ the fluid and rock

are assumed to have the same temperature.

The advective mass flux ($\mathbf{F}_M$) is

$$\mathbf{F}_M = \rho \mathbf{u} = -\frac{k\rho}{\mu}\left(\nabla P - \rho \mathbf{g}\right), \tag{2.4}$$

where **u** is the Darcian velocity, $k$ is permeability, $\mu$ is viscosity, $P$ is pressure, and **g** is the vector of gravitational acceleration.

The conductive and convective heat flux ($\mathbf{F}_H$) is

$$\mathbf{F}_H = -\lambda \nabla T + h\mathbf{F}_M, \tag{2.5}$$

where $\lambda$ is the thermal conductivity and $h$ is the specific enthalpy.

### 2.2.2. Simulation model development

A heat pump is located indoors and moves heat from indoor air to the circulating fluid using mechanical work. A fluid pump sends the circulating fluid through the BHE and a heat pump. A BHE transfers heat to the ground. Figure 2.1 is a schematic diagram of the vertical closed-loop GHP system in cooling mode.

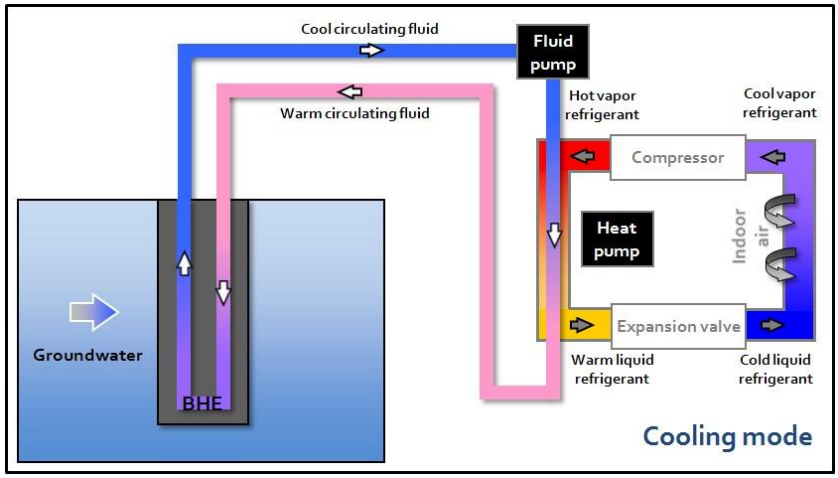


(a)

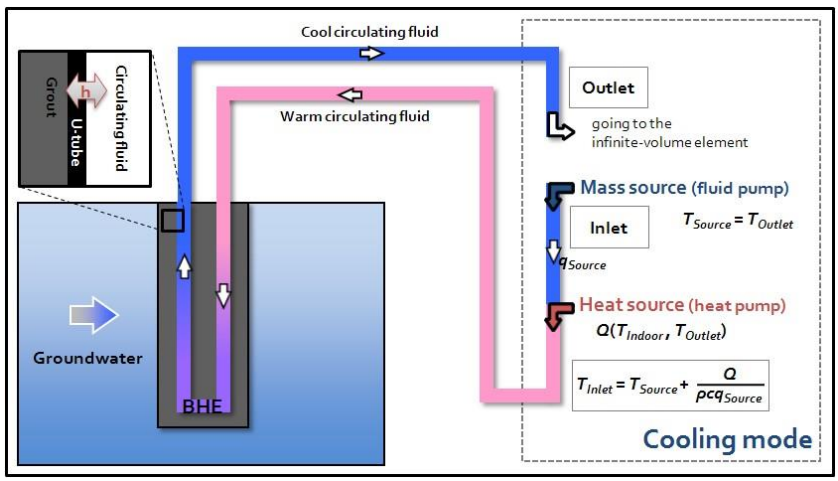


(b)

**Figure 2.1.** Schematic diagram of the vertical closed-loop GHP system: (a) real system and (b) model conceptualization. The heat pump moves heat from indoor air to the circulating fluid, the fluid pump sends the circulating fluid through the BHE and heat pump, and the BHE transfers heat to the ground for cooling operation.

The simulation model presented in this study focuses on the temperature variations in the circulating fluid and in the vicinity of the BHE. The simulator is based on a widely accepted three-dimensional numerical simulator for heat and fluid flow in geothermal systems, TOUGHREACT. TOUGHREACT can consider fluid flow occurring under viscous, pressure, and gravity forces according to Darcy's law and heat transport by means of conduction and convection including both sensible and latent heat transport. To take thermal and hydraulic processes related to the vertical closed-loop GHP system into account, three modules are developed and added to TOUGHREACT (Figure 2.1b). The developed simulator is referred to as the modified TOUGHREACT.

The first module calculates heat flux across the interface between the circulating fluid and the U-tube wall in the BHE. The surface of the U-tube wall is warmer/cooler than the circulating fluid in the heating/cooling seasons so that heat/cold is being transferred from the U-tube wall to the circulating fluid. Then the heat transfer coefficient is used for calculating the heat transfer between the flowing fluid and the solid wall. The heat flux ($\mathbf{F}_H$) between the fluid and the wall is

$$\boldsymbol{F}_H = -h\left(T_w - T_f\right), \tag{2.6}$$

where $h$ is the heat transfer coefficient, $T_w$ is the temperature of the U-tube wall, and $T_f$ is the bulk temperature of the circulating fluid. The bulk temperature is used on the assumption that the circulating fluid is well mixed (i.e., all at the same temperature) across each cross-section of the U-tube. The $h$ is not a constant but a

variable, depending on the fluid velocity and properties, the system geometry, and the temperature of the fluid and the wall (Bird et al., 1960). The *h* is often calculated from the

$$\text{Nusselt number } Nu = \frac{h\left(T_w - T_f\right)}{\lambda_f \frac{\left(T_w - T_f\right)}{d}} = h\frac{d}{\lambda_f}, \tag{2.7}$$

where *d* is the pipe diameter and $\lambda_f$ is the thermal conductivity of the fluid. The *Nu* is the ratio of the total to conductive heat transfer between the fluid and the pipe wall. A classical expression for computing the local Nusselt number for fully developed turbulent flow in a smooth circular tube is of the form

$$Nu = C\,\mathrm{Re}^m\,\mathrm{Pr}^n,$$

$$\mathrm{Re} = \frac{vd\rho}{\mu},$$

$$\mathrm{Pr} = \frac{\rho\mu}{\lambda}, \tag{2.8}$$

where *C*, *m*, and *n* are constants determined experimentally. Re and Pr denote the Reynolds number and Prandtl number, respectively. Dittus and Boelter (1930) suggested that $C = 0.0243$, $m = 0.8$, and $n = 0.4$ for heating of the fluid and $C = 0.0265$, $m = 0.8$, and $n = 0.3$ for cooling of the fluid, by using the experimental values of Morris and Whitman (1928). Now it has become common practice to refer to following equation as the Dittus–Boelter equation (Incropera et al., 2007; Winterton, 1998).

$$Nu = 0.023 Re^{0.8} Pr^{n}, \quad (2.9)$$

where n = 0.4 for heating and 0.3 for cooling.

The second module considers the fluid pump. TOUGHREACT cannot simulate circulation of the fluid in a closed circuit. To simulate such circulation, the mass source term in Eq. (2.1) and an infinite-volume element are used. A mass source term at the inlet in Figure 2.1 generates a fluid with a temperature the same as that of the fluid at the BHE outlet ($T_{\text{Source}} = T_{\text{Outlet}}$). This fluid passes through the BHE to the BHE outlet, where it flows into an infinite-volume element that has no effect on the other elements and simulation results, effectively acting as a mass sink.

The third module calculates the rate of energy transfer between the heat pump and circulating fluid. The energy transfer rate, $Q$ in Figure 2.1b, depends on the type of heat pump, indoor air temperature ($T_{Indoor}$), and circulating fluid temperature at the BHE outlet ($T_{Outlet}$). The thermal and electric power of the heat pump varies with the $T_{Indoor}$ and $T_{Outlet}$. The variation data can be obtained from the specification data sheet of the heat pump. Table 2.1 is an example of a specification data sheet for a heat pump. The $P_T$ is the thermal power carried by the heat pump and the $P_E$ is the electric power supplied to operate the heat pump.

If the type of heat pump is known and the $T_{Indoor}$ fixed at some value, then the $P_T$, $P_E$, and $Q$ in the current time step can be updated because the $T_{Outlet}$ is already known from the results of the previous time step. Using the $T_{Source}$ and updated energy transfer rate $Q$ as a heat source, the $T_{Inlet}$ at the current time step is calculated:

$$T_{Inlet} = T_{Source} + \frac{Q}{\rho c q_{Source}}, \tag{2.10}$$

where $c$ is the specific heat of the circulating fluid and $q_{Source}$ is the flow rate of the circulating fluid.

The coefficient of performance for the heating mode ($COP_H$) or for the cooling mode ($COP_C$), which are often used to quantify the efficiency of a GHP system, can also be evaluated by this module. The COP is the ratio of the output thermal power ($P_T$) to the input electric power ($P_E$) at a given operating point:

$$COP = \frac{P_T}{P_E}. \tag{2.11}$$

TOUGH2 and its descendants such as TOUGHREACT are based on the integral finite-difference (IFD) method (Edwards, 1972; Narasimhan and Witherspoon, 1976). Contrary to typical finite-difference methods, the IFD method has the advantage of irregular discretization in multiple dimensions. Spatial discretization is accomplished by a developed grid generator. It generates an IFD grid and input files that are suitable for simulating the vertical closed-loop GHP system in the modified TOUGHREACT. Figure 2.2 illustrates an IFD grid used in simulations of both the sensitivity analysis on parameters of BHE design and the evaluation of BHE performance.

**Table 2.1.** Example of the specification data sheet: cooling and heating capacity data for the heat pump FHP EM015 made by FHP manufacturing. The $T_{Outlet}$ is the circulating fluid temperature at the BHE outlet, the $T_{Indoor}$ is the indoor air temperature, the $P_T$ is the thermal power carried by the heat pump, the $P_E$ is the electric power supplied to operate the heat pump, the $Q$ is the energy transfer rate, and the $COP_C$ and $COP_H$ are the coefficients of performance for the cooling mode ($COP_C$) and for the heating mode ($COP_H$), respectively.

| | $T_{Outlet}$ (°C) | $T_{Indoor}$ (°C) | $P_T$ (kW) | $P_E$ (kW) | $Q$ (kW) | $COP_C$ (-) |
|---|---|---|---|---|---|---|
| Cooling capacity data | 15.6 | 23.9 | 4.40 | 1.04 | 5.45 | 4.2 |
| | 21.1 | | 4.21 | 1.14 | 5.35 | 3.7 |
| | 29.4 | | 3.92 | 1.29 | 5.21 | 3.0 |
| | 37.8 | | 3.63 | 1.44 | 5.07 | 2.5 |
| | 15.6 | 29.4 | 5.27 | 1.06 | 6.32 | 5.0 |
| | 21.1 | | 5.03 | 1.16 | 6.19 | 4.3 |
| | 29.4 | | 4.69 | 1.31 | 6.00 | 3.6 |
| | 37.8 | | 4.34 | 1.46 | 5.80 | 3.0 |
| | $T_{Outlet}$ (°C) | $T_{Indoor}$ (°C) | $P_T$ (kW) | $P_E$ (kW) | $Q$ (kW) | $COP_H$ (-) |
| Heating capacity data | 10.0 | 15.6 | 4.78 | 1.29 | 3.49 | 3.7 |
| | 15.6 | | 5.53 | 1.35 | 4.17 | 4.1 |
| | 21.1 | | 6.27 | 1.42 | 4.85 | 4.4 |
| | 26.7 | | 7.02 | 1.49 | 5.53 | 4.7 |
| | 10.0 | 21.1 | 4.52 | 1.31 | 3.21 | 3.5 |
| | 15.6 | | 5.23 | 1.38 | 3.85 | 3.8 |
| | 21.1 | | 5.93 | 1.45 | 4.48 | 4.1 |
| | 26.7 | | 6.64 | 1.51 | 5.12 | 4.4 |

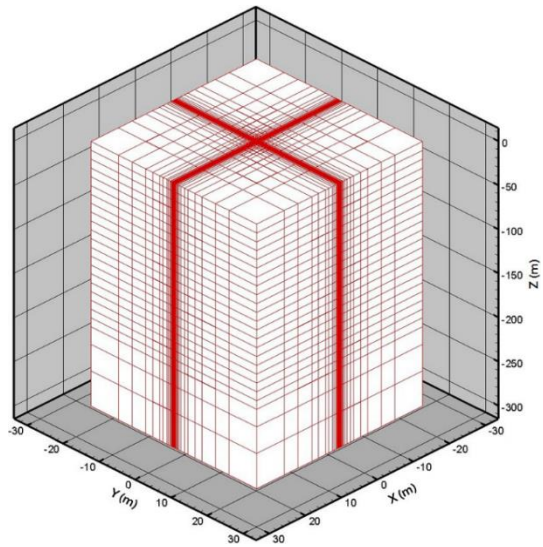


(a)

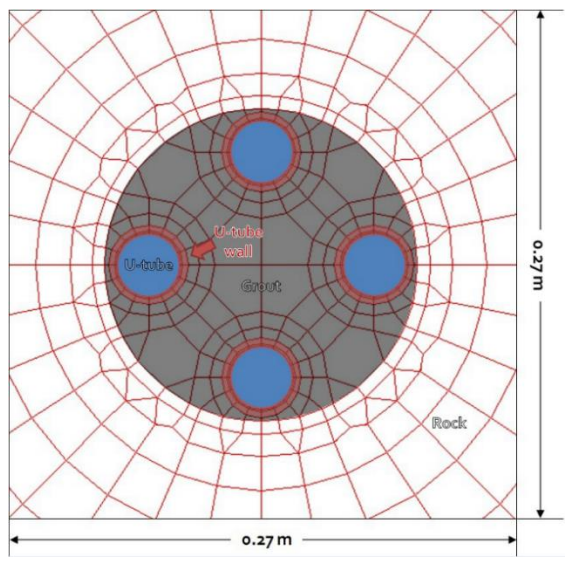


(b)

**Figure 2.2.** IFD grid: (a) complete model domain (*x* to *z* ratio of 5) and (b) plan view at the periphery of the BHE. A detailed shape of the cross-section of the BHE is shown clearly.

## 2.3. Study area

The Korean government began supporting research into low-enthalpy geothermal utilization systems in 2003 (Shim et al., 2006). As a result of government funding, a vertical closed-loop GHP system and its monitoring system were installed in the building of the Earthquake Research Center (ERC) at the Korea Institute of Geoscience and Mineral Resources (KIGAM) in Daejeon, Korea, and they have operated and been monitored since 2006 (Figure 2.3). The vertical closed-loop GHP system comprises 79 heat pumps, 4 fluid pumps, and 28 BHEs. There are 16, 31, and 32 heat pumps on the first, second, and third floors of the ERC building, respectively. Three fluid pumps supply the circulating fluid to the heat pumps on each floor and to the BHEs. The fourth fluid pump is an auxiliary fluid pump. There are 8, 10, and 10 BHEs connected to the heat pumps on the first, second, and third floors, respectively under the yard of the ERC building. The dimensions of the BHE field are 35 m from east to west and 42 m from north to south. Each BHE consists of a closed circuit with a double U-tube in a grouted borehole 200 m deep. To measure the temperature and flow rate of the circulating fluid at the BHE inlet and outlet, monitoring equipment has been installed for three BHEs. Figure 2.4 represents the layout of the GHP and its monitoring system for the ERC building.

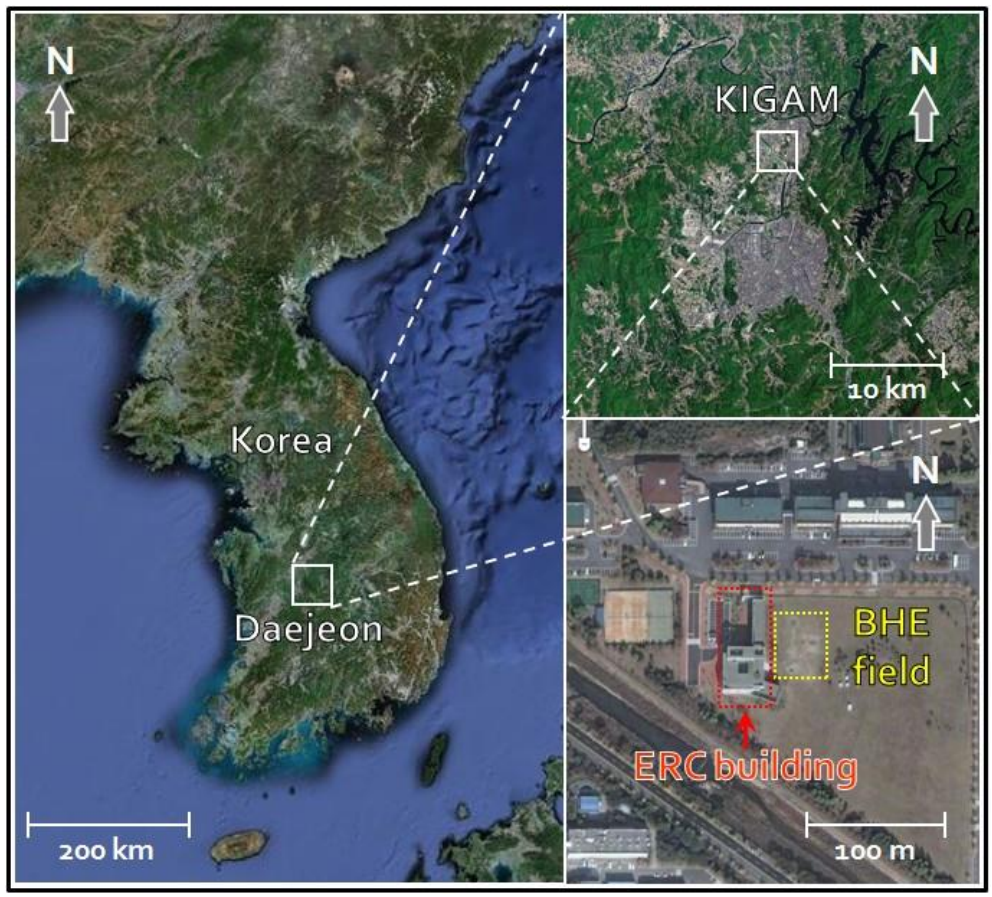


**Figure 2.3.** Map of the study area. A vertical closed-loop GHP system and its monitoring system were installed in the ERC building at the KIGAM in Daejeon, Korea.

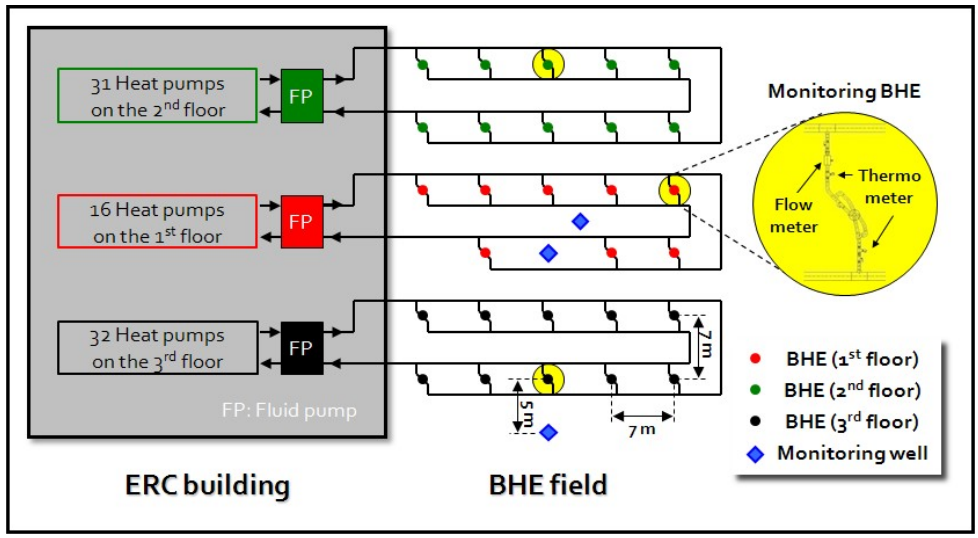


**Figure 2.4.** Layout of the GHP and its monitoring system in the ERC building. The vertical closed-loop GHP system comprises 79 heat pumps, 4 fluid pumps, and 28 BHEs. The dimensions of the BHE field are 35 m from east to west and 42 m from north to south.

To characterize geologic, hydrogeologic, and geothermal parameters, several surveys were carried out at this site (Shim et al., 2006; Kim and Lee, 2007). The geology of the site mainly consists of Jurassic Nampo Group sedimentary rocks and Daebo granite. The density, specific heat, and thermal diffusivity of the rock matrix were measured on 61 core samples from a 300 m deep monitoring well on the south side of the BHE field. The harmonic means of the parameters are 2.67 $g/cm^3$, 0.82 kJ/kgK, and 1.37 $mm^2/s$, respectively. The specific heat and thermal diffusivity of the rock matrix were measured by the LFA-447 Xenon flash lamp machine from Netzsch, and the density of the rock matrix was measured by the AccuPyc 1330 Pycnometer from Micromeritics Instrument Corporation. The thermal conductivity of the core samples was estimated from these data. The thermal gradient of 20℃/km was measured in the 300 m monitoring well. The basal heat flow of 59.7 $mW/m^2$ was estimated from the harmonic mean of thermal conductivity of 2.98 W/mK and the thermal gradient. A packer test for determination of the hydraulic conductivity was conducted for every 3 m section of the 300 m monitoring well. The hydraulic conductivities are in the range of $1.0 \times 10^{-4}$ to $1.0 \times 10^{-8}$ m/s. The characteristics of the BHE, heat pump, and rock are summarized in Table 2.2.

**Table 2.2.** Characteristics of the BHE, heat pump, and rock.

| | | |
|---|---|---|
| **Borehole heat exchanger** | Dimensions | Number of BHEs: 1F (8), 2F (10), 3F (10)<br>Depth: 200 m<br>Spacing between BHEs: 7 m<br>Borehole radius: 82.5 mm<br>U-tube radius (inner): 17 mm<br>U-tube radius (outer): 21 mm |
| | Thermal conductivity (W/mK) | U-tube: 0.366 (Polyethylene pipe)<br>Grout: 0.800 (Sand–E-plug mixture)<br>Circulating fluid: 0.580 (Water) |
| | Specific heat (kJ/kgK) | U-tube: 2.09<br>Grout: 2.20<br>Circulating fluid: 4.20 |
| **Heat pump** | Type | FHP EM Series<br>(EM012, EM015, EM024, EM028, EM041) |
| | Number of heat pumps | 1F: EM024 (9), EM028 (5), EM041 (2)<br>2F: EM012 (11), EM015 (16), EM024 (3), EM028 (1)<br>3F: EM012 (10), EM015 (17), EM024 (4), EM028 (1) |
| **Rock** | Flow properties | Porosity: 0.014<br>Hydraulic conductivity: $1.0 \times 10^{-4}$ to $1.0 \times 10^{-8}$ m/s |
| | Thermal properties | Thermal conductivity: 2.98 W/mK (harmonic mean)<br>Specific heat: 0.82 kJ/kgK (harmonic mean)<br>Density: 2.67 g/cm$^3$ (harmonic mean) |

## 2.4. Model setup and validation

### 2.4.1. Model setup

The domain dimensions used in numerical simulations are set as 45 m in both horizontal directions and 300 m in the vertical direction from the ground surface, which are sufficiently large to avoid boundary effects. Boundary conditions are listed in Table 2.3. The diurnal and interseasonal variations of the ground surface temperature are not considered in the simulation. Instead of, annual mean ground surface temperature is used in the simulation. The unsaturated zone near the ground surface is ignored and assumed to be saturated zone in the simulation. If it is considered in the simulation, the computational load is increased significantly. The effect of it on the vertical closed-loop system is usually negligible in Korea because its depth is much smaller than the depth of the BHE. In the KIGAM GHP system, its depth is in the range of 3 to 10 m. On the contrary, it can have a great effect on the SCW and open-loop system, because they use the groundwater directly. Then, the groundwater recharge by rain or snow melt also should be considered in the simulation of these systems. To assemble the governing mass- and energy-balance equations, the thermos-physical properties of fluid mixtures needed are provided by equation-of-state (EOS) modules in TOUGH2 and its descendants (Pruess et al., 1999). The various EOS modules included in the package of TOUGH2 and its descendants can represent different fluid mixtures. EOS1 is used in this model, which

is the most basic EOS module, providing a description of pure water in its liquid, vapor, and two-phase states.

### 2.4.2. Model validation

Validation of the modified TOUGHREACT proceeds by comparing two actual datasets with their respective simulation results. One dataset comprises the results of a thermal response test (Gehlin, 2002) that was carried out at one of the BHEs in the ERC building from November 21 to November 29, 2007. The thermal response test began with an average thermal power of 10 kW for 74 hours. The average flow rate of the circulating fluid was about 37 L/min. After heat injection for 74 hours, no heat was applied to the circulation fluid, but the fluid circulation and temperature monitoring were continued for about 5 days. Using the modified TOUGHREACT model, a numerical simulation was carried out using the parameters and conditions in Tables 2.2 and 2.3. Figure 2.5 shows that the simulated results are in good agreement with the results of the thermal response test.

**Table 2.3.** Boundary conditions for the BHE simulations.

| | | |
|---|---|---|
| **Boundary conditions** | **Hydraulic** | Constant head: left and right sides<br>(hydraulic gradient: 0.02)<br>No flow: the others<br>Constant flow rate: BHE inlet (flow rate: 0.5 L/s) |
| | **Thermal** | Constant temp.: top (15℃)<br>Constant flux: bottom (basal heat flow: 59.7 mW/m$^2$)<br>Constant temp.: lateral sides (depth-dependent) |

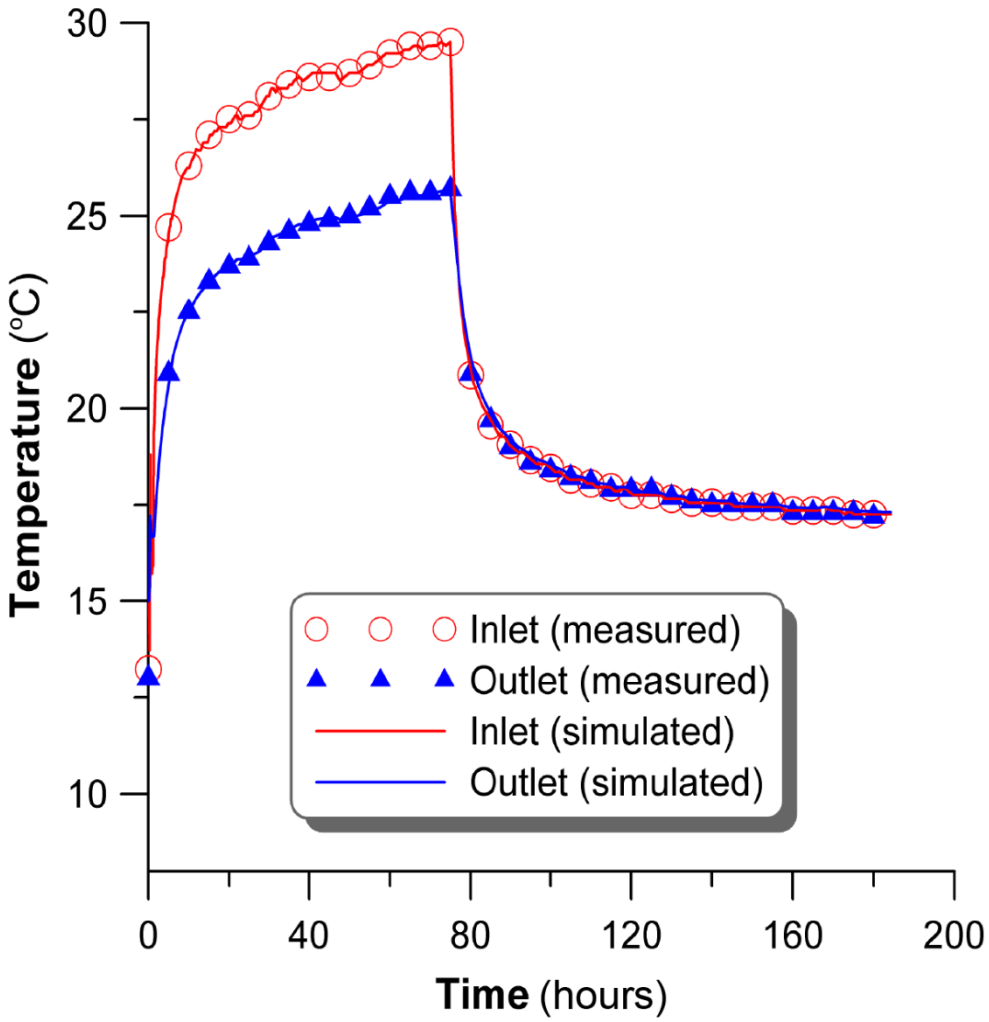


**Figure 2.5.** Validation of the developed model: comparisons of simulated and measured temperatures at the inlet and outlet of the BHE during the thermal response test.

The other dataset is an operational dataset for the ERC building. Data were recorded for the three monitoring BHEs (see Figure 2.3) during the summer and winter of 2006. Only the data taken from the first and second floors during winter 2006 are used to verify the proposed model because of the poor continuity in the data recorded during summer 2006 and because of trouble with the thermometer on the third floor during winter 2006. From November 27 to December 26, 2006, the inlet temperature, outlet temperature, and flow rate of the circulating fluid were monitored every 20 minutes. Using the temperature difference between the inlet and outlet of the BHE and the flow rate of the circulating fluid, the rate of the energy transfer from the heat pumps to the circulating fluid is calculated. Simulated inlet and outlet temperatures are compared with the monitored inlet and outlet temperatures of the first and second floors in Figures 2.6a and 2.6b, respectively. The simulated inlet and outlet temperatures are in good agreement with the monitored inlet and outlet temperatures of both floors. The root mean squared error (RMSE) is 0.18℃ at the inlet and 0.14℃ at the outlet of the first floor, and 0.22℃ at the inlet and 0.18℃ at the outlet of the second floor. The normalized RMSE is 0.043 at the inlet and 0.044 at the outlet of the first floor, and 0.050 at the inlet and 0.064 at the outlet of the second floor.

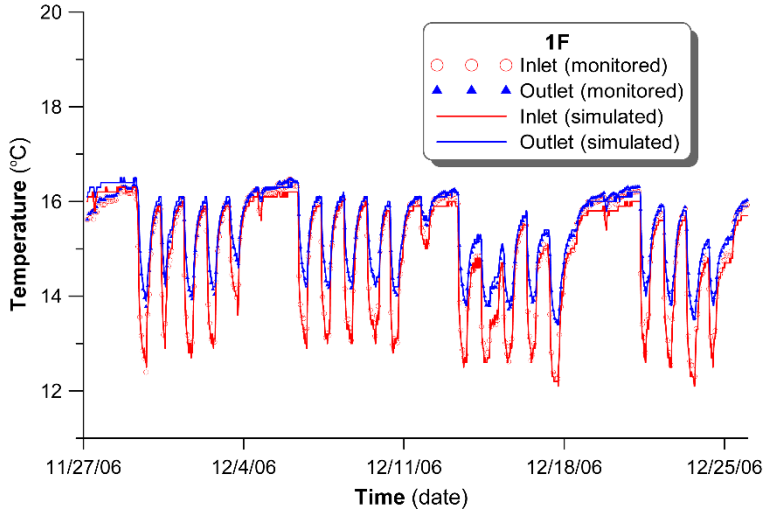


(a)

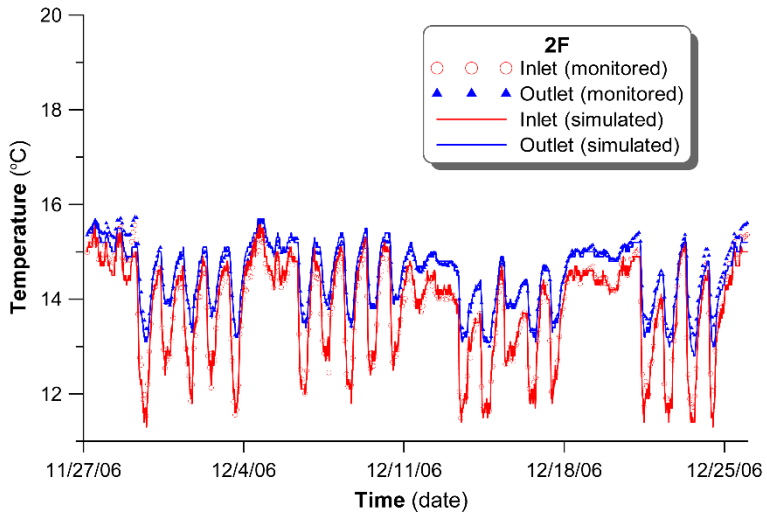


(b)

**Figure 2.6.** Comparisons of simulated temperatures and monitored temperatures at the inlet and outlet of the BHE during four weeks of operation: (a) first floor and (b) second floor.

The developed simulation model is validated both using a dataset with a simple load condition (the thermal response dataset) and a dataset with a complex load condition (the operational dataset). The simulation results are in good agreement with both measurement datasets. Therefore, the simulation model can be applied to various problems such as sensitive analysis of properties affecting the performance of the BHE and design evaluation for finding the optimal number of BHEs to minimize installation and operation costs.

## 2.5. Sensitivity analysis

The developed simulation model is applied to analyze the sensitivities of design parameters that can affect the performance of the BHE. Seven parameters that can affect performance of the GHP system are used for sensitivity analysis. Figure 2.7b shows seven parameters and those ranges used in the sensitivity analysis. The distribution range of parameters that are related to the ground is determined by considering acceptable range in the realm of nature. The range of the others that are made by industrial processes is determined by the material property of them. The reference value for each parameter is underlined in Figure 2.7b. A thermal power of 5 kW is assumed to be injected to the circulating fluid during 90 days. Flow rate of the circulating fluid is given as 0.5 L/s.

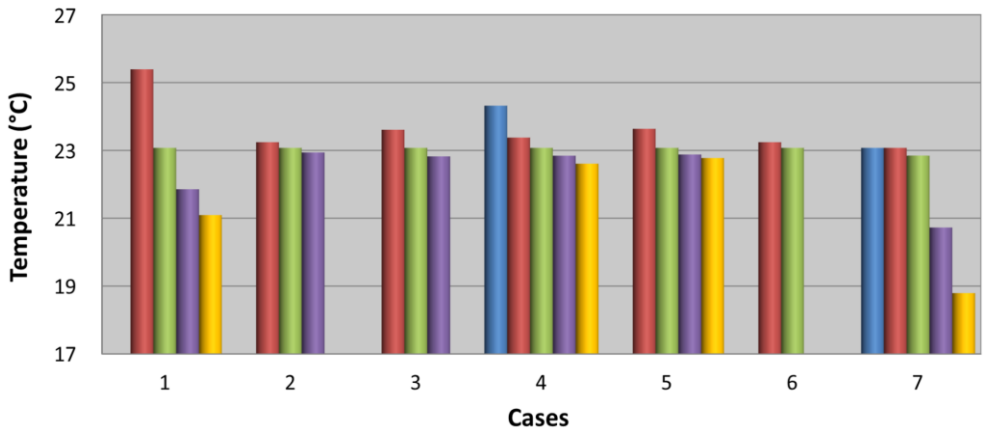


(a)

| | | | | | | |
|---|---|---|---|---|---|---|
| 1 | Thermal conductivity of the ground (W/m-K) | - | 2 | 3 | 4 | 5 |
| 2 | Heat capacity of the ground (kJ/kg-K) | - | 0.4 | 0.8 | 1.2 | - |
| 3 | Density of the ground (g/cm$^3$) | - | 1 | 2.65 | 4 | - |
| 4 | Thermal conductivity of the grout (W/m-K) | 0.27 | 0.55 | 0.8 | 1.2 | 2.38 |
| 5 | Thermal conductivity of the U-tube (W/m-K) | - | 0.1 | 0.366 | 0.7 | 2 |
| 6 | Heat transfer coefficient (kW/m$^2$-K) | - | 0.32 | 1.07 | - | - |
| 7 | Hydraulic conductivity (m/s) | $10^{-9}$ | $10^{-7}$ | $10^{-5}$ | $10^{-4}$ | $10^{-3}$ |

(b)

**Figure 2.7.** Results of sensitivity analysis: (a) average temperature of the circulating fluid at the outlet of borehole heat exchanger during a 90-day heat injection and (b) seven parameters and those ranges used in the sensitivity analysis.

Figure 2.7a shows average temperature of the circulating fluid at the BHE outlet during a 90-day heat injection period. The most sensitive parameter on the performance of the BHE is the thermal conductivity of the ground. The maximum temperature difference of the circulating fluid at the BHE outlet is about 3.7℃ when the thermal conductivity of the ground is changed from 2 W/m-K to 5 W/m-K. When the thermal conductivity of the ground is only changed from 2 W/m-K to 3 W/m-K, then temperature difference of the circulating fluid at the BHE outlet is about 2.3℃. This is remarkable difference because areas where the thermal conductivity of the ground is less than 2 W/m-K can be easily found. The next most sensitive parameter on the performance of the BHE is the hydraulic conductivity of the groundwater or Darcian velocity of the groundwater. The heat transfer coefficient and the specific heat of the aquifer have hardly effect on the performance of the BHE. If the thermal conductivity of the grout is not too low, its effect on the performance of the BHE is insignificant. Therefore, thermal conductivity of the ground should be measured for designing BHEs properly.

## 2.6. BHE design evaluation

Using the developed simulation model, a numerical evaluation of the design of the KIGAM BHE system is carried out. The evaluation procedure involves (1)

establishing criteria and guidelines for the design evaluation, (2) simulating the base case, (3) simulating modified cases, and (4) cost analysis. The base case is that there exist 8, 10, and 10 BHEs connected to heat pumps on the first, second, and third floors, respectively. The modified case is that a series of BHEs connected to heat pumps on each floor are changed from the base case.

### 2.6.1. Criteria and guidelines for the design evaluation

*2.6.1.1. Criteria*

*2.6.1.1.1. Temperature.* The temperature of the circulating fluid at the BHE outlet should be within the range from –4 to 43℃ described on the specification data sheet of the heat pump. Circulating fluid that is too hot (or too cold) may result in heat pumps breaking down or not working.

*2.6.1.1.2. Efficiency.* The COP is a widely used index when evaluating efficiency of heat pumps. For example, closed-loop ENERGY STAR® -labeled geothermal heat pumps must meet two criteria: the $COP_H$ must exceed 3.3 and the $COP_C$ must exceed 4.13. These criteria are established for certain test conditions in which the air flow rate, fluid flow rate, entering air temperature, and entering fluid temperature are fixed.

*2.6.1.1.3. Cost analysis.* Because GHP systems are basically developed to save

electricity and its cost, an analysis of financial profit and loss is important. By comparing construction cost with operation cost, the most cost-effective case can be found.

*2.6.1.2. Guidelines*

The rate of energy transfer between the heat pump and the circulating fluid, Q depends on characteristics of the heat pumps, operation pattern, temperature of the circulating fluid ($T_{Outlet}$), and indoor temperature ($T_{Indoor}$). Characteristics of the heat pumps can be obtained from the specification data sheet from manufactures for each heat pump (Table 2.1). The hypothetical operation pattern is obtained in accordance with the calculating method specified in Annex 4, Korean Agency for Technology and Standards 9306, 1999. The total number of operation days is 90 days for the cooling and heating seasons individually. The operation time per day is 12 hours and the operating ratio for the operation period is 0.6 for the base case. For the modified cases, the operating ratio is automatically controlled to hold the thermal power ($P_T$) of the heat pumps as a constant. For example, if the number of BHEs is decreased, the temperature of the circulating fluid increases in the cooling season. To then hold the $P_T$ of heat pumps as a constant, the operating ratio is increased because the efficiency of the heat pump decreases.

There are many heat pumps in the KIGAM GHP system, and the operation timings of the heat pumps differ. If the operation ratio of each heat pump is 0.6, the

number of operating heat pumps at a specific time can be assumed to be 60% of the total number of heat pumps. Therefore, the energy transfer rate is 60% of the overall energy transfer rate. The indoor temperature is set at 28℃ during the cooling season and at 18℃ during the heating season, which are the indoor temperatures recommended for Korean public institutions by the Korean government.

One representative BHE among all BHEs connected to heat pumps on each floor is considered in simulations under the assumption that the temperatures of the circulating fluids in the BHEs are about the same, regardless of the BHEs. Boundary conditions, initial conditions, aquifer parameters, and other parameters are the same as those in previous simulations.

### 2.6.2. Simulation results for the base case

Table 2.4 presents the results of numerical simulations for the base case. $|\mathbf{\Delta T}|$ represents the absolute value of the temperature difference between the $T_{Inlet}$ and $T_{Outlet}$ (℃). All values listed in Table 2.4 are averaged over all heat pumps on each floor and over the whole operation period.

**Table 2.4.** Results of numerical simulations for the base case. The $T_{Inlet}$ and $T_{Outlet}$ are the circulating fluid temperatures at the BHE inlet and outlet, respectively, the **|ΔT|** is the absolute value of temperature difference between the $T_{Inlet}$ and $T_{Outlet}$, and the $COP_C$ and $COP_H$ are the coefficients of performance for the cooling mode ($COP_C$) and for the heating mode ($COP_H$), respectively.

| **Season** | **Floor** | $P_T$ **(kW)** | $P_E$ **(kW)** | $T_{Inlet}$ **(°C)** | $T_{Outlet}$ **(°C)** | **\|ΔT\| (°C)** | **$COP_C$ (-)** | **$COP_H$ (-)** |
|---|---|---|---|---|---|---|---|---|
| Cooling season | 1F | 83.3 | 18.0 | 29.73 | 26.15 | 3.58 | 4.64 | – |
| | 2F | 89.3 | 22.4 | 28.46 | 24.99 | 3.47 | 3.99 | – |
| | 3F | 94.1 | 23.7 | 28.95 | 25.49 | 3.46 | 3.98 | – |
| Heating season | 1F | 79.0 | 18.7 | 9.51 | 11.64 | 2.13 | – | 4.23 |
| | 2F | 90.5 | 23.9 | 10.28 | 12.34 | 2.06 | – | 3.79 |
| | 3F | 95.3 | 25.1 | 9.99 | 12.04 | 2.05 | – | 3.80 |

Using the $P_T$ and $P_E$ , the $COP_C$ and $COP_H$ are obtained. The $COP_C$ of heat pumps on the first floor is 16.3% and 16.6% higher than the $COP_C$s on the second and third floors, respectively. The $COP_H$ of heat pumps on the first floor is 11.6% and 11.3% higher than $COP_H$s on the second and third floors, respectively. The reason for these different values is not that the number of BHEs connected to the first floor are more than the number of BHEs connected to the other floors, but that heat pumps on the first floor are more efficient. The temperature of the circulating fluid in the first-floor BHEs is higher (lower) than that of the circulating fluid in the second-floor and third-floor BHEs for the cooling (heating) season.

The $COP_H$s of heat pumps on the first and second floors, which are obtained from the monitoring data used in the model verification, are 4.40 and 3.89, respectively. Differences between the $COP_H$s from the monitoring data and the $COP_H$s from the simulation data are 3.86% on the first floor and 2.57% on the second floor. This suggests that the hypothetical operation pattern is suitable for the evaluation of the KIGAM GHP system. The reason that the $COP_H$ determined from the monitoring data is higher than the $COP_H$ determined from the simulation data seems to be that there are unused and empty offices in the ERC building.

Figure 2.8 shows an example of the temperature field in and around a BHE after 90 days of operation. It is a result of the base case for the first floor. Groundwater flows from left to right in the figure. A thermal plume downstream and temperature difference between the BHE inlet and outlet can be seen in both seasons.

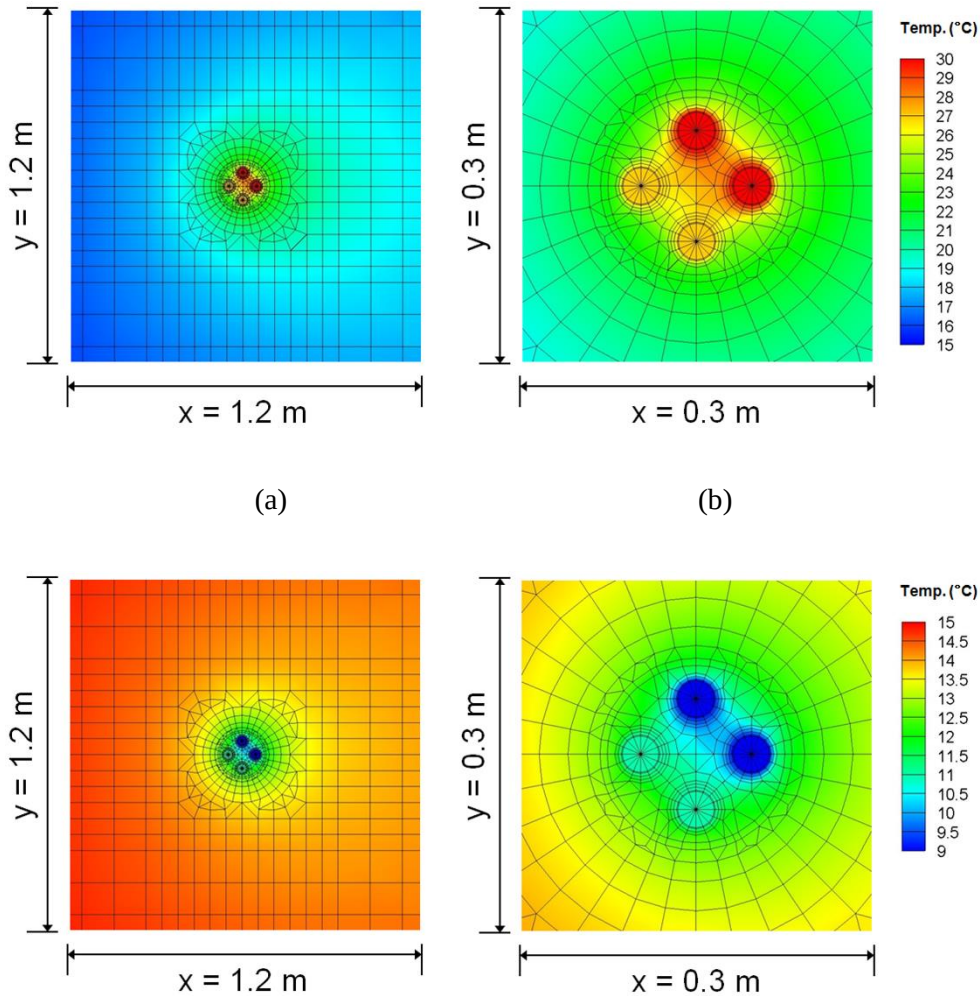


**Figure 2.8.** Plan view of temperature field in and around the BHE on the ground surface after 90 days of operation: (a) cooling season, (b) cooling season (zoomed view), (c) heating season, and (d) heating season (zoomed view).

### 2.6.3. Simulation results for the modified cases

Requiring that a given number of BHEs produces the same $P_T$ obtained from the base case determines the operating ratio (OR) for each case. The OR is varied with the $T_{Outlet}$ and automatically adjusted at every time step (Table 2.5). Here, $MT_{Outlet}$ represents the maximum (in the cooling season) or minimum (in the heating season) temperature of the circulation fluid at the BHE outlet (℃). In all cases, $MT_{Outlet}$ is within the range in which heat pumps can be operated without problems arising. The OR is found to be in the range of 0.57 to 0.70. The range of variation of the OR in the heating season is larger than that in the cooling season because the $P_T$ in the heating season is more sensitive to variations in $T_{Outlet}$ than is $P_T$ in the cooling season. The range of variation of the $p_e$ in the cooling season, however, is larger than that in the heating season. Though the $P_T$ in the cooling season is nearly the same as the $P_T$ in the heating season, more energy is transferred from heat pumps to the circulating fluid in the cooling season than is transferred in the heating season (see **|ΔT|** in Table 2.5). The more transferred energy, the greater temperature change in the circulating fluid. The $P_E$ is affected by both the OR and $T_{Outlet}$, with $T_{Outlet}$ having the greater effect.

**Table 2.5.** Results of numerical simulations for cases in which the number of BHEs is modified. The OR is the operating ratio, $MT_{Outlet}$ represents the maximum (in the cooling season) or minimum (in the heating season) temperature of the circulation fluid at the BHE outlet, and the COP is the coefficients of performance.

| | Number of BHEs | $P_T$ (kW) | OR | $P_E$ (kW) | $T_{Inlet}$ (℃) | $T_{Outlet}$ (℃) | $\|\Delta T\|$ (℃) | $MT_{Outlet}$ (℃) | COP |
|---|---|---|---|---|---|---|---|---|---|
| **1F (cooling season)** | 4 | 83.3 | 0.65 | 22.9 | 41.15 | 37.40 | 3.75 | 42.08 | 3.64 |
| | 6 | 83.3 | 0.61 | 19.5 | 33.41 | 29.78 | 3.63 | 32.70 | 4.28 |
| | 8 | 83.3 | 0.6 | 18.0 | 29.73 | 26.15 | 3.58 | 28.25 | 4.64 |
| | 10 | 83.3 | 0.59 | 17.1 | 27.60 | 24.05 | 3.55 | 25.66 | 4.86 |
| | 12 | 83.3 | 0.58 | 16.6 | 26.21 | 22.68 | 3.53 | 24.02 | 5.01 |
| **1F (heating season)** | 4 | 79.0 | 0.7 | 20.6 | 3.63 | 5.68 | 2.05 | 3.17 | 3.84 |
| | 6 | 79.0 | 0.63 | 19.3 | 7.51 | 9.62 | 2.11 | 7.84 | 4.10 |
| | 8 | 79.0 | 0.6 | 18.7 | 9.51 | 11.64 | 2.13 | 10.27 | 4.23 |
| | 10 | 79.0 | 0.58 | 18.4 | 10.72 | 12.86 | 2.14 | 11.74 | 4.30 |
| | 12 | 79.0 | 0.57 | 18.2 | 11.53 | 13.67 | 2.14 | 12.71 | 4.35 |
| **2F (cooling season)** | 6 | 89.3 | 0.63 | 26.0 | 35.09 | 31.51 | 3.58 | 34.86 | 3.43 |
| | 8 | 89.3 | 0.61 | 23.7 | 30.88 | 27.37 | 3.51 | 29.75 | 3.77 |
| | 10 | 89.3 | 0.6 | 22.4 | 28.46 | 24.99 | 3.47 | 26.82 | 3.99 |
| | 12 | 89.3 | 0.59 | 21.6 | 26.89 | 23.45 | 3.44 | 24.94 | 4.13 |
| | 14 | 89.3 | 0.58 | 21.1 | 25.78 | 22.36 | 3.42 | 23.61 | 4.24 |
| **2F (heating season)** | 6 | 90.5 | 0.66 | 25.4 | 6.82 | 8.83 | 2.01 | 6.92 | 3.56 |
| | 8 | 90.5 | 0.62 | 24.4 | 8.97 | 11.01 | 2.04 | 9.53 | 3.71 |
| | 10 | 90.5 | 0.6 | 23.9 | 10.28 | 12.34 | 2.06 | 11.12 | 3.79 |
| | 12 | 90.5 | 0.58 | 23.6 | 11.16 | 13.23 | 2.07 | 12.18 | 3.84 |
| | 14 | 90.5 | 0.57 | 23.3 | 11.79 | 13.87 | 2.08 | 12.96 | 3.88 |
| **3F (cooling season)** | 6 | 94.1 | 0.63 | 27.7 | 35.97 | 32.40 | 3.57 | 35.93 | 3.40 |
| | 8 | 94.1 | 0.61 | 25.1 | 31.51 | 28.01 | 3.50 | 30.52 | 3.75 |
| | 10 | 94.1 | 0.6 | 23.7 | 28.95 | 25.49 | 3.46 | 27.44 | 3.98 |
| | 12 | 94.1 | 0.59 | 22.8 | 27.27 | 23.84 | 3.43 | 25.43 | 4.13 |
| | 14 | 94.1 | 0.58 | 22.2 | 26.10 | 22.69 | 3.41 | 24.02 | 4.25 |
| **3F (heating season)** | 6 | 95.3 | 0.66 | 26.8 | 6.34 | 8.34 | 2.00 | 6.35 | 3.56 |
| | 8 | 95.3 | 0.62 | 25.7 | 8.61 | 10.64 | 2.03 | 9.08 | 3.71 |
| | 10 | 95.3 | 0.6 | 25.1 | 9.99 | 12.04 | 2.05 | 10.76 | 3.80 |
| | 12 | 95.3 | 0.58 | 24.7 | 10.91 | 12.98 | 2.07 | 11.88 | 3.86 |
| | 14 | 95.3 | 0.57 | 24.5 | 11.58 | 13.65 | 2.07 | 12.70 | 3.90 |

Figure 2.9 shows the variations in the $COP_C$ and $COP_H$ according to changes in the number of BHEs. If the number of BHEs decreases, the $COP_C$ and $COP_H$ decrease rapidly, and if the number of BHEs increases, the $COP_C$ and $COP_H$ increase slowly, because the $COP_C$ and $COP_H$ are in inverse proportion to the $P_E$. The $COP_C$ is more sensitive to change in the number of BHEs than the $COP_H$ is.

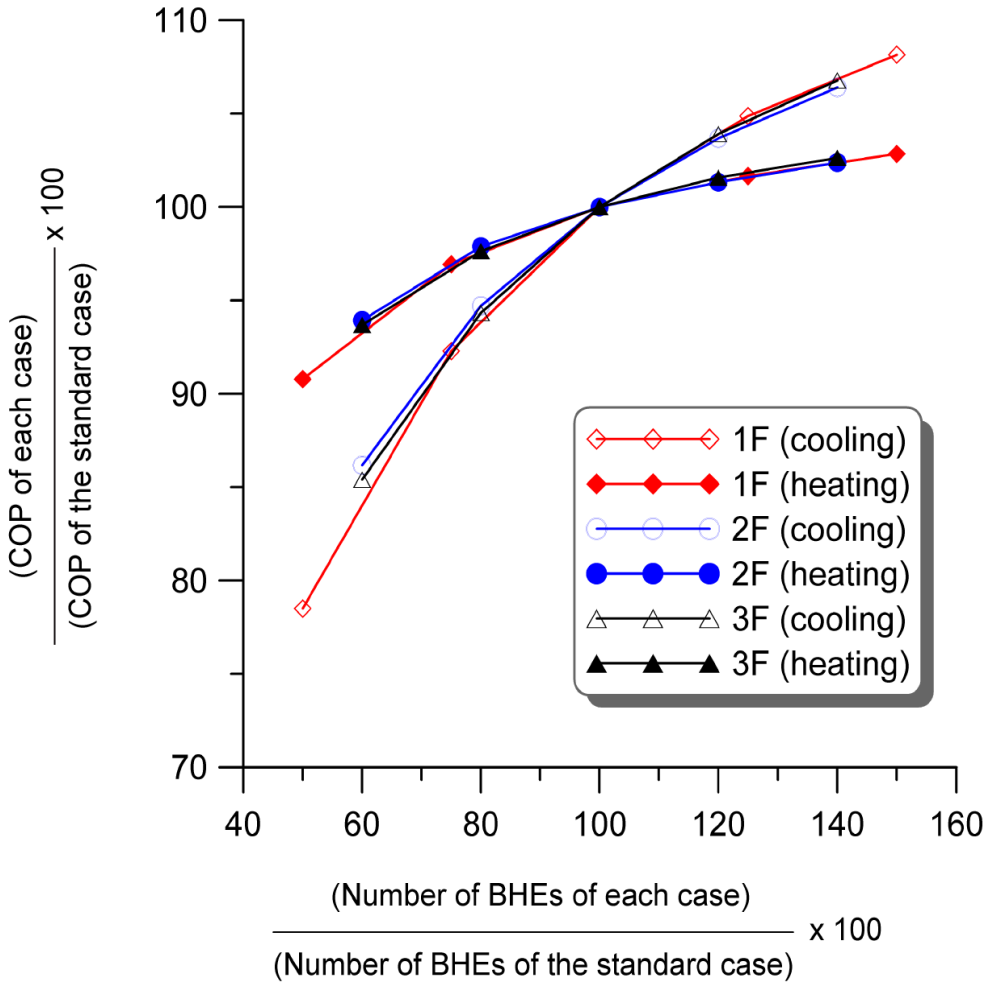


**Figure 2.9.** Variation in the $COP_C$ or $COP_H$ with a change in the number of BHEs. The $COP_C$ is more sensitive to change in the number of BHEs than the $COP_H$ is.

### 2.6.4. Cost analysis

The construction cost of one BHE in the KIGAM GHP system was about US$8000. The lifetime of a BHE is assumed to be 25 years and the cost of electricity to vary between 0.1 and 1 US$/kWh, and calculate the most suitable number of BHEs. The cost of electricity in Korea at present is about 0.1 US$/kWh. A prediction of the variation in the electric bill is not easy because it is related to oil and uranium prices, carbon dioxide emission restrictions, and other factors. If the cost of electricity does not change for the next 25 years, it is most cost-effective for there to be 4, 6, and 6 BHEs for the first, second, and third floors, respectively (Figure 2.10). If the average cost of electricity for the next 25 years is 1 US$/kWh, it is most cost-effective to have 12, 14, and 14 BHEs for the first, second, and third floors, respectively. If the average cost of electricity for the next 25 years is 0.4 US$/kWh, the base case is the most cost-effective.

The predicted cost of electricity in the year 2030 is 0.146 US$/kWh and the estimated average cost of electricity for the next 25 years is 0.123 US$/kWh. The predictions are based on the extrapolation of electricity cost data collected by the Korean National Statistical Office from 1975 to 2008. In this case, it would be most cost-effective to have 4, 6, and 6 BHEs for the first, second, and third floors, respectively.

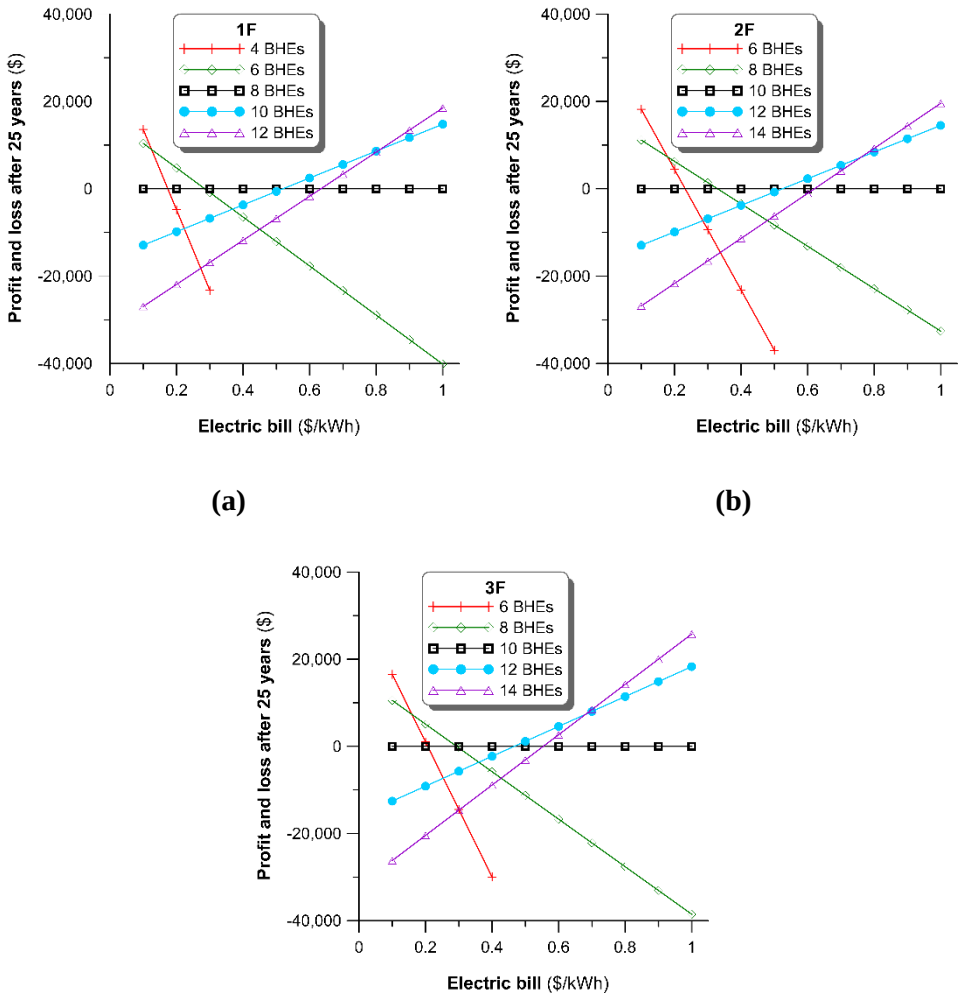


**Figure 2.10.** Economic profit and loss after 25 years according to changes in the cost of electricity: (a) first floor, (b) second floor, and (c) third floor.

## 2.7. Summary and conclusion

A model that can estimate the performance of a vertical closed-loop GHP system was developed and verified. The model was applied to analyze the sensitivities of design parameters that can affect the performance of the BHEs and in evaluating the KIGAM GHP system. The most sensitive parameters on the performance of the BHEs are the thermal conductivity of aquifer and the Darcian groundwater velocity considering acceptable distribution range in the realm of nature. To simulate a vertical closed-loop GHP system, three modules are added to TOUGHREACT. The modules enable us to calculate the heat transfer between the U-tube and circulating fluid, consider the circulation of the circulating fluid in the BHE, and calculate the rate of energy transfer from a heat pump to a BHE. The developed simulation model was validated using the measurement and monitoring datasets. The respective simulation results are in good agreement with the two datasets. Using the developed simulation model, the BHE design of the KIGAM BHE system was numerically evaluated. For the base case, the $COP_C$s and $COP_H$s of heat pumps on the first, second, and third floors are 4.64 and 4.23, 3.99 and 3.79, and 3.98 and 3.80, respectively. For the modified cases, the $COP_C$s and $COP_H$s of heat pumps on the first, second, and third floors are in the ranges of 3.64–5.01 and 3.84–4.35, 3.43–4.24 and 3.56–3.88, and 3.40–4.25 and 3.56–3.90, respectively. The predicted cost of electricity in 2030 is 0.146 US$/kWh. The most cost-effective

system in this case is to 4, 6, and 6 BHEs on the first, second, and third floors, respectively. The BHEs of the KIGAM GHP system seem to be overdesigned unless electricity costs quadruple. The overdesigned system is financially unattractive over many years, and then one of the main reason for using the GHP system, saving money, is removed.

The developed simulation model can be used to suggest quantitative data for the sizing of BHEs when the type and number of heat pumps are already determined. The output of the model, such as the temperature of the circulating fluid, efficiency of the heat pump, and economic profit and loss of the GHP system, can be useful in reducing the initial cost, avoiding oversizing or undersizing of the GHP system, and ensuring the efficiency of the GHP system.

# Chapter 3. Simulation modeling of multiple borehole heat exchangers and evaluation of the long-term performance of the vertical closed-loop geothermal heat pump system

## 3.1. Introduction

In this chapter, a new simulator and grid generator is developed to simulate the vertical closed-loop GHP system that consists of multiple BHEs. The developed simulation model in chapter 2 can only consider one BHE. Massively parallel computing procedures into the serial simulator are introduced for the multi-BHE system. Parallel computing improves distributing memory requirements and computational efficiency for solving large simulation problems with a great number of grid-blocks. Thus, the base simulator of the simulation model is changed to TOUGH2-MP, a massively parallel version of the TOUGH2 code, instead of TOUGHREACT. TOUGH2-MP is also modified to be able to simulate the vertical closed-loop GHP system. The new grid generator is designed to produce a simulation domain with multiple BHEs.

The newly developed simulation model can consider thermal interactions between BHEs when the system is in operation and thermal storage in the ground after the operation period of the system. The heat/cold released from the BHE can be transferred to other BHEs by conduction or convection. This thermal interactions between BHEs have a negative effect on the performance of the BHE. The temperature around the BHE field after the cooling/heating season is higher/lower than the initial temperature. The stored heat/cold in the ground can remain near the BHE field until the next heating/cooling season unless the ground is fully recovered thermally. It has a positive effect on the performance of the BHE. These two mechanisms should be considered in the evaluation of long-term performance of the BHE.

The developed simulation model is tested for the performance improvement through parallelization. The model is then applied to evaluate the performance of the KIGAM GHP system for a 25-year operation.

## 3.2. Method

Zhang et al. (2008) developed TOUGH2-MP that is designed to perform parallel simulation on multi-CPU computational platforms for improving modeling capabilities significantly in terms of problem size and simulation time. A simulation domain (Figure 3.1a) is subdivided into a number of subdomains in performing a

parallel simulation. The partitioning algorithm from the MTEIS software package (Karypsis and Kumar, 1998) is used for subdividing the domain automatically and effectively. The partitioned subdomains are assigned to each processor for updating thermophysical properties, assembling mass and energy balance equations, solving linear equation systems, and performing other local computations (Figure 3.1b). Parallel simulations are run as multiple processors simultaneously and MPI (Message-Passing Interface; Message Passing Forum, 1994) is employed for data communications between processors (Figure 3.1c). Aztec linear solver package (Tuminaro et al., 1999) is used for solving the linear equation systems assigned to each processor in parallel. After solving local linear equation systems during each Newton iteration step, the entire linear equation system is solved together by all processors collaboratively via communication between neighboring (Figure 3.1b).

The contents of modification is similar to in the previous chapter, on the contrary, the procedure of modifying TOUGH2-MP is much more complicated because of the parallel implementation than the procedure of modifying TOUGHREACT. Figure 3.2 is a new schematic diagram of the vertical closed-loop GHP system with three core components. Three modules are developed and added to TOUGH2-MP to consider thermal and hydraulic processes related to the three core components of the system, i.e. BHEs, heat pumps, and fluid pumps, respectively. The developed simulator is referred to as the mT2MP.

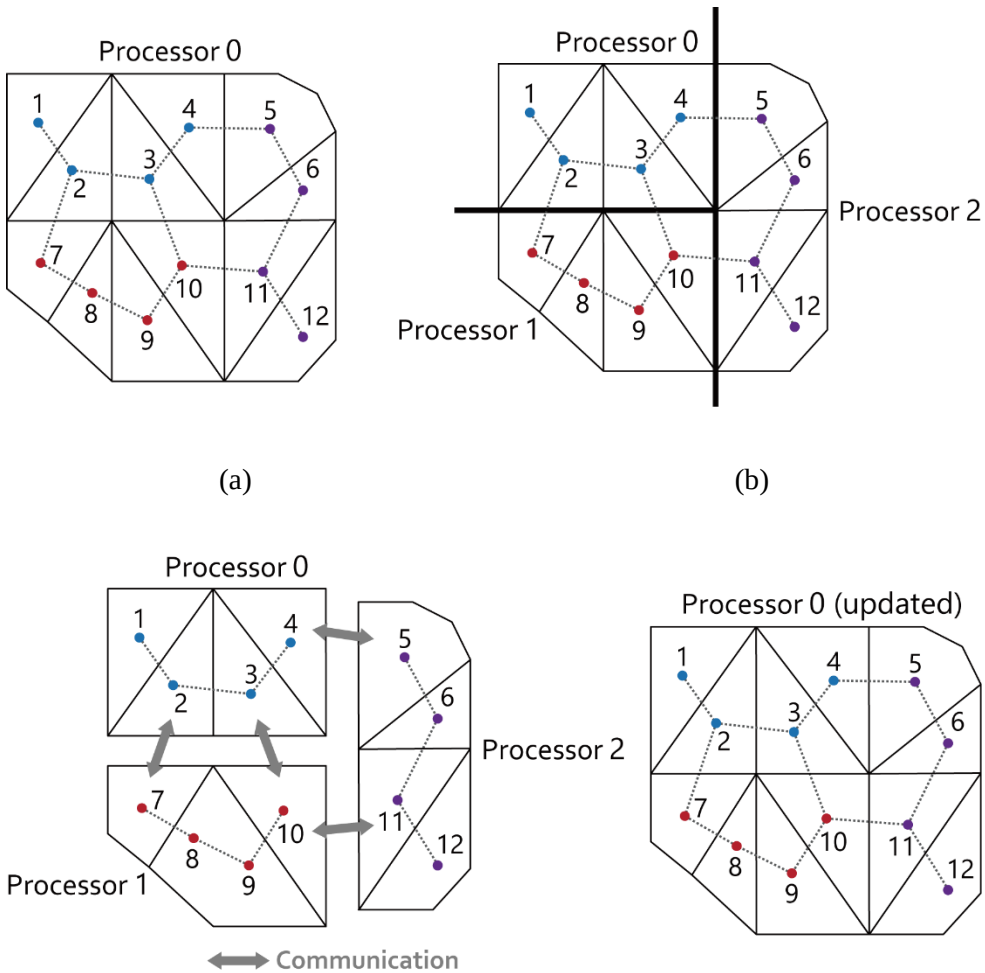


**Figure 3.1.** An example of domain partitioning and parallel computing implementation: (a) a 12-elements domain, (b) partitioning on 3 processors, (c) computation on each processor and communication with each other, (d) state variable update.

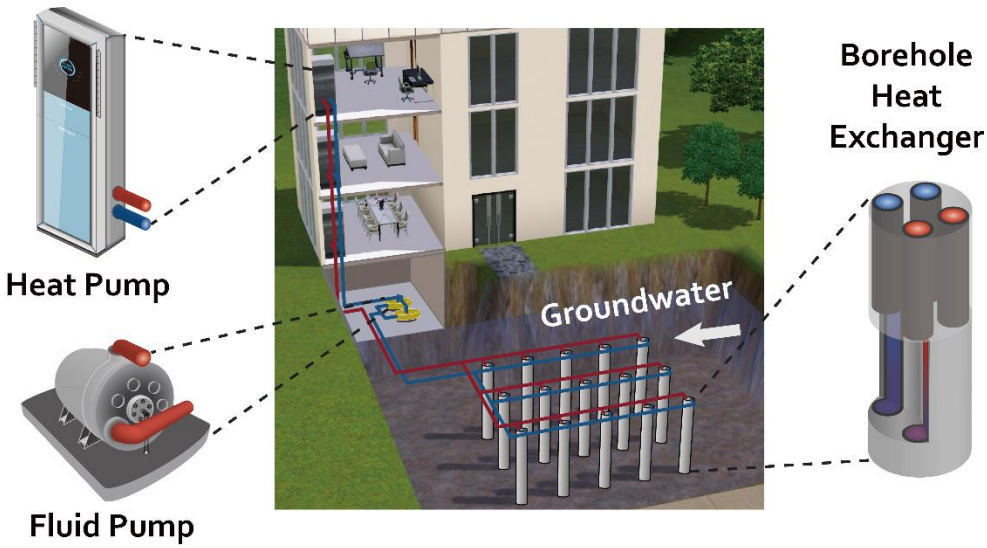


**Figure 3.2.** Schematic diagram of the vertical closed-loop GHP system with three core components. Simulations of the vertical closed-loop GHP system that consists of multiple BHEs can be feasible.

The first module is developed for the BHEs. The heat transfer coefficient in Eq. (2.6) is also used in calculating the convective heat transfer between the circulating fluid and U-tube wall. The temperature of the circulating fluid at the outlet of each BHE ($T_{out}1$, $T_{out}2$, and $T_{out}3$ in Figure 3.3) can be different from each other because the performance of the BHE depends on its location and surrounding environment. The circulating fluid is gathered and flows to the pipe(s) connected to the fluid pump(s) in the building. The mean temperature of the gathered circulating fluid, $T_{avr}$, is

$$T_{avr} = \frac{\sum_{m=1}^{N_{BHE}} T_{out}m}{N_{BHE}}, \tag{3.1}$$

where $N_{BHE}$ is the number of BHEs and $T_{out}m$ is the temperature of the circulating fluid at the outlet of the m-th BHE. If the heat pump system is composed of more than one group, such as the KIGAM GHP system, the mean temperature of the gathered circulating fluid of the n-th group, $T_{avr}n$, is

$$T_{avr}n = \frac{\sum_{m=1}^{N_{BHE}n} T_{out}m,n}{N_{BHE}n}, \tag{3.2}$$

where $N_{BHE}n$ is the number of BHEs of the n-th group and $T_{out}m,n$ is the temperature of the circulating fluid at the outlet of the m-th BHE of the n-th group.

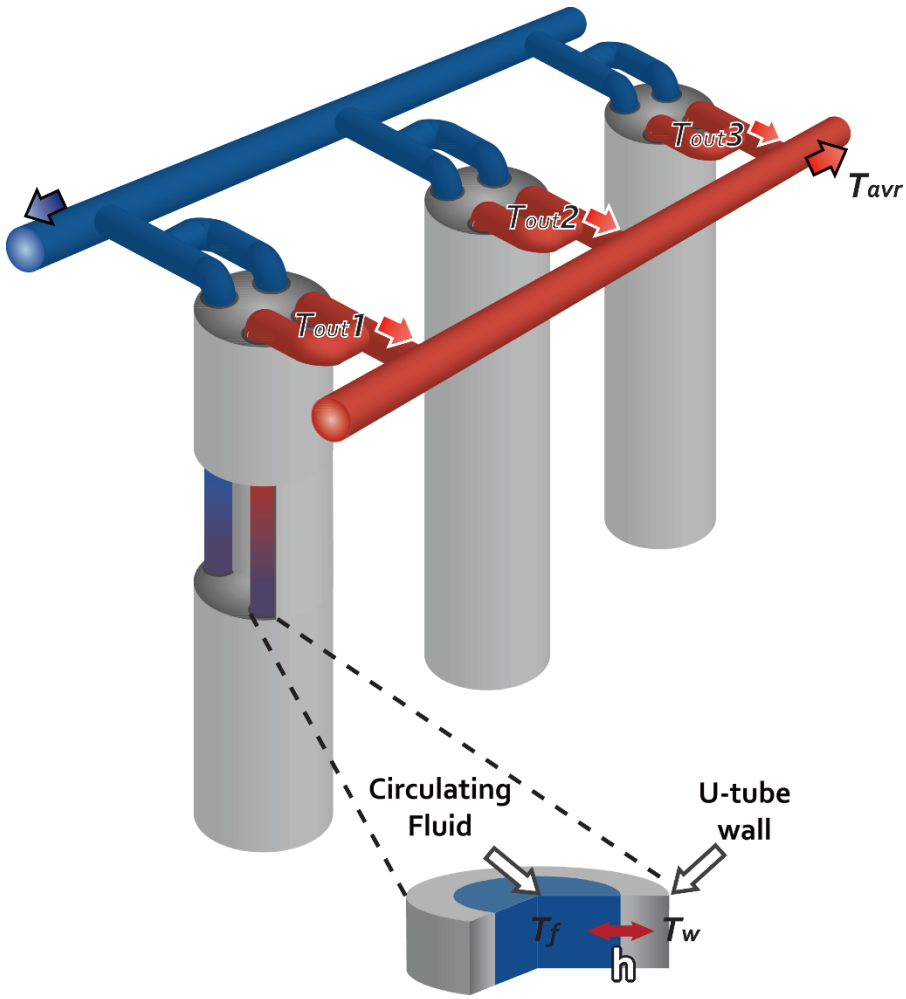


**Figure 3.3.** Schematic diagram of multiple BHEs. The temperature of the circulating fluid at the outlet of each BHE ($T_{out}1$, $T_{out}2$, and $T_{out}3$) can be different from each other. The mean temperature of the gathered circulating fluid, $T_{avr}$, is needed for simulations of the vertical closed-loop GHP system that consists of multiple BHEs. The heat transfer coefficient, h in Eq. (2.6), is used in calculating the convective heat transfer between the circulating fluid and U-tube wall.

The second module is developed for the fluid pumps and almost identical to the second module of the modified TOUGHREACT. A mass source term generate a fluid with a temperature the same as the $T_{avr}$ (Figure 3.4a). An infinite-volume element in Figure 3.4b is effectively acting as a mass sink, which has no effect on the other elements and simulation results. If the heat pump system is composed of n groups, then the number of mass source terms is n.

The third module is developed for the heat pump. The heat pump compresses the refrigerant to make it hotter on the side to be warmed, and releases the pressure at the side where heat is absorbed (Figure 3.5b). It is activated only when the room temperature is lower/higher than the set temperature in the heating/cooling season. If the $T_{avr}$ and the room temperature ($T_{indoor}$) are known, the specification data sheet of the heat pump (Table 3.1) can provide the thermal power carried by the heat pump from the indoor air ($p_{HP\text{-}indoor}$), the electric power supplied to operate the heat pump ($p_{electric}$), and the thermal power between the heat pump and circulating fluid ($p_{HP\text{-}CF}$). The $T_{indoor}$ can be obtained from the outdoor temperature, heat insulation properties of the room, and heat source or sink in the room. When the heat pump is in operation, then the $p_{HP\text{-}CF}$ can be calculated from the $T_{avr}$ and $T_{indoor}$. When the heat pump is stopped, then the $p_{HP\text{-}CF}$ is zero. These parameters are updated in each time step of the simulation. In the case that the $T_{indoor}$ and current operating state of the heat pump are unknown, the $p_{HP\text{-}CF}$ can be estimated by assuming that the $T_{indoor}$ is a constant and adopting the operating ratio ($OR$). The temperature of the circulating fluid after it passed through the heat pump, $T_{in}$, is:

$$T_{in} = T_{avr} + OR\frac{\sum_{m=1}^{N_{HP}} p_{HP-CF}m}{q_{CF}C_{CF}}, \quad (3.3)$$

where the $N_{HP}$ is the number of heat pumps, $p_{HP\text{-}CF}m$ ($Q$ in table 2.1) is the thermal power between the m-th heat pump and circulating fluid, $q_{CF}$ is the flow rate of the circulating fluid, and $C_{CF}$ is the specific heat of the circulating fluid. The $OR$ is 1 in the case that the current operating state of the heat pump is known. It is set to a certain value between 0 and 1 and will be automatically adjusted to maintain the cooling/heating performance of the heat pump in the case that the current operating state of the heat pump is unknown. For example, if the $T_{avr}$ is increased in the cooling season, then the operating ratio is increased to hold the $p_{HP\text{-}indoor}$ constant. It means that the heat pump is in operation for longer periods because the efficiency of the heat pump is decreased.

The coefficient of performance for the heating mode ($COP_H$) or for the cooling mode ($COP_C$), which are often used to quantify the efficiency of a GHP system, can also be evaluated by this module. The COP is the ratio of the $p_{HP\text{-}indoor}$ to the $p_{electric}$ at a given operating point:

$$\mathrm{COP} = \frac{p_{HP-indoor}}{p_{electric}}, \quad (3.4)$$

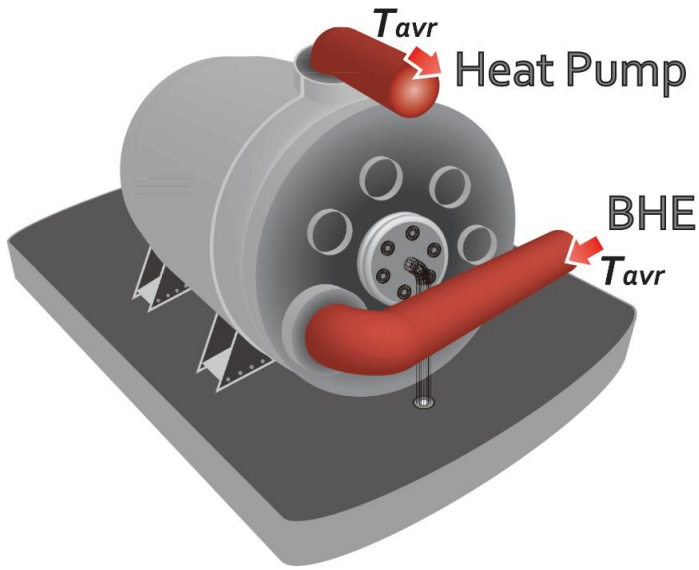


(a)

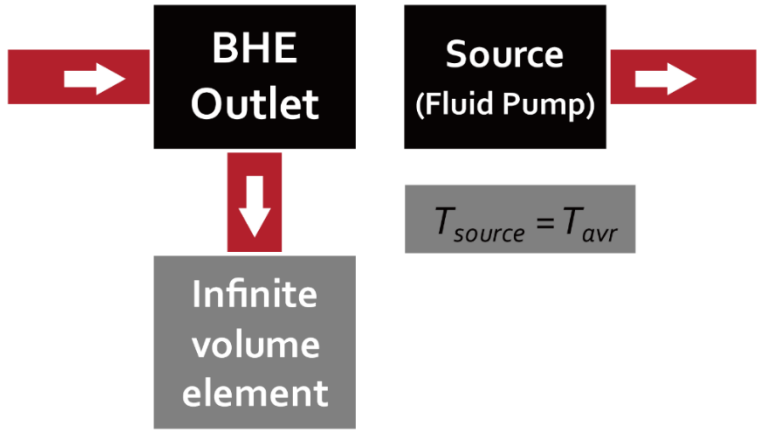


(b)

**Figure 3.4.** Schematic diagram of the fluid pump: (a) real fluid pump and (b) model conceptualization. A mass source term generate a fluid with a temperature the same as the $T_{avr}$. An infinite-volume element is effectively acting as a mass sink

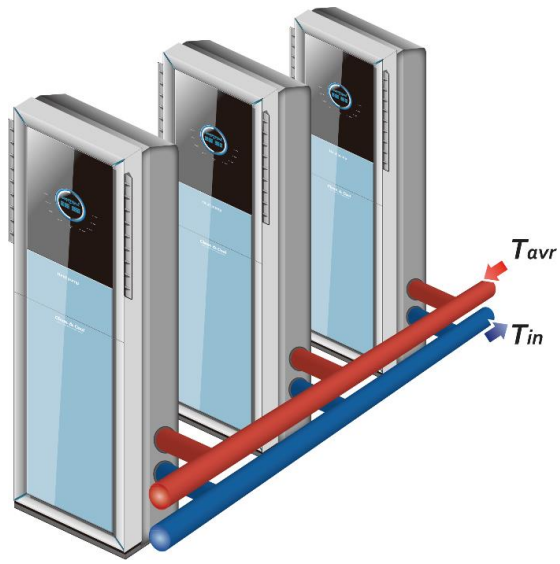


(a)

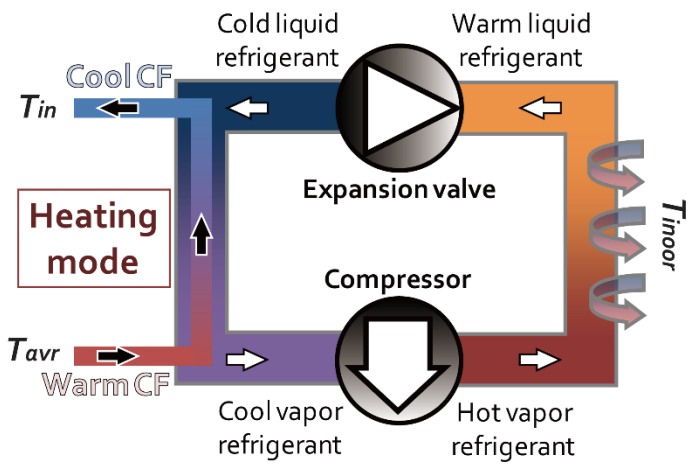


(b)

**Figure 3.5.** Schematic diagram of the heat pump: (a) real heat pump and (b) model conceptualization. The heat pump compresses the refrigerant to make it hotter on the side to be warmed, and releases the pressure at the side where heat is absorbed.

**Table 3.1.** Example of the specification data sheet: cooling and heating capacity data for the heat pump FHP EM015 made by FHP manufacturing. The $T_{avr}$ is the average temperature of the gathered circulating fluid, the $T_{Indoor}$ is the room temperature, the $p_{HP\text{-}indoor}$ is the thermal power carried by the heat pump from the indoor air, the $p_{electric}$ is the electric power supplied to operate the heat pump, the $p_{HP\text{-}CF}$ is the thermal power between the heat pump and circulating fluid, and the $COP_C$ and $COP_H$ are the coefficients of performance for the cooling mode ($COP_C$) and for the heating mode ($COP_H$), respectively.

| | $T_{avr}$ (°C) | $T_{Indoor}$ (°C) | $p_{HP\text{-}indoor}$ (kW) | $p_{electric}$ (kW) | $p_{HP\text{-}CF}$ (kW) | $COP_C$ (-) |
|---|---|---|---|---|---|---|
| **Cooling capacity data** | 15.6 | 23.9 | 4.40 | 1.04 | 5.45 | 4.23 |
| | 21.1 | | 4.21 | 1.14 | 5.35 | 3.69 |
| | 29.4 | | 3.92 | 1.29 | 5.21 | 3.04 |
| | 37.8 | | 3.63 | 1.44 | 5.07 | 2.52 |
| | 15.6 | 29.4 | 5.27 | 1.06 | 6.32 | 4.97 |
| | 21.1 | | 5.03 | 1.16 | 6.19 | 4.34 |
| | 29.4 | | 4.69 | 1.31 | 6.00 | 3.58 |
| | 37.8 | | 4.34 | 1.46 | 5.80 | 2.97 |
| | $T_{avr}$ (°C) | $T_{Indoor}$ (°C) | $p_{HP\text{-}indoor}$ (kW) | $p_{electric}$ (kW) | $p_{HP\text{-}CF}$ (kW) | $COP_H$ (-) |
| **Heating capacity data** | 10.0 | 15.6 | 4.78 | 1.29 | 3.49 | 3.7 |
| | 15.6 | | 5.53 | 1.35 | 4.17 | 4.1 |
| | 21.1 | | 6.27 | 1.42 | 4.85 | 4.4 |
| | 26.7 | | 7.02 | 1.49 | 5.53 | 4.7 |
| | 10.0 | 21.1 | 4.52 | 1.31 | 3.21 | 3.5 |
| | 15.6 | | 5.23 | 1.38 | 3.85 | 3.8 |
| | 21.1 | | 5.93 | 1.45 | 4.48 | 4.1 |
| | 26.7 | | 6.64 | 1.51 | 5.12 | 4.4 |

## 3.3. Speedup test

Zhang et al. (2008) showed that the TOUGH2-MP code can provide significant gains in computational efficiency. Figure 3.6a shows that a linear or super-linear speedup can be obtained for different numbers of processors and for different parts of the simulation. The parallel code shows much better performance than ideal linear speedup, which can be understood in terms of efficiency obtainments from decomposing one large linear algebra problem into a series of smaller ones.

The developed simulation model, mT2MP, and the original TOUGH2-MP code are tested on a Linux cluster equipped with 8 nodes using a gigabit Ethernet switch connection, and each node consists of an Intel quad-core 3.4 GHz CPU. For testing the parallel code performance, the model was run using either 2, 4, 8, 16, or 32 processors for the same simulation time period. Figure 3.6b that a linear speedup can be obtained from both the modified and original TOUGH2-MP code for different numbers of processors. Although the super-linear speedup cannot be obtained because of the number of processors on the Linux cluster is insufficient, the computational efficiency of the developed simulation model is considerably increased in direct proportion to the number of the processors.

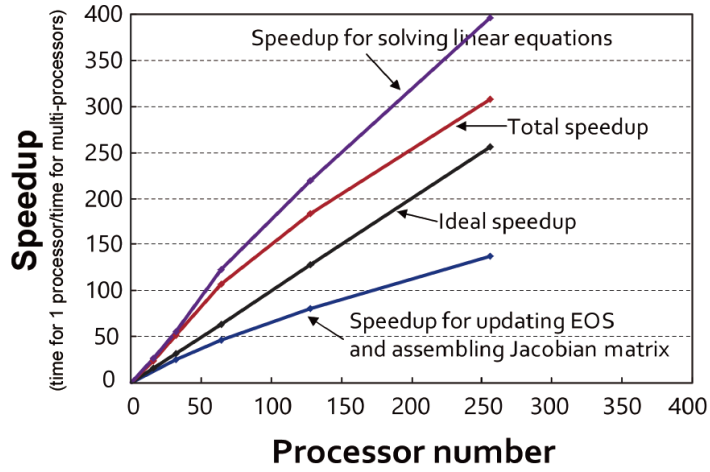


(a)

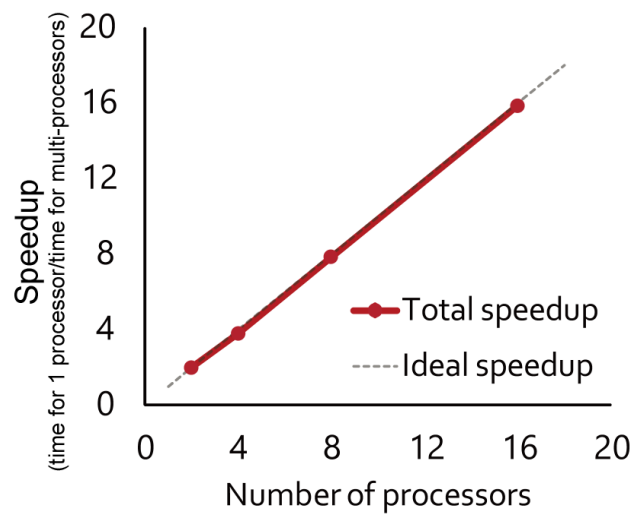


(b)

**Figure 3.6.** Speedup (ratio of simulation time for one processor to simulation time for multi-processors) for the parallel simulations of the (a) original and (b) modified TOUGH2-MP.

## 3.4. Evaluation of the long-term performance of the KIGAM GHP system

### 3.4.1. Study area

The KIGAM GHP system introduced in the previous chapter is located in Daejeon, Korea (Figure 3.7a). It is separated into three groups corresponded to each floor of the ERC building. The first group consists of 31 heat pumps on the second floor, one fluid pump, and 10 BHEs at the upper side of the BHE field. The second group consists of 16 heat pumps on the first floor, one fluid pump, and 8 BHEs at the middle of the BHE field. The third group consists of 32 heat pumps on the third floor, one fluid pump, and 10 BHEs at the lower side of the BHE field (Figure 3.7c). Each group has one monitoring BHE equipped with two thermometers and one flow meter (Figure 3.7b). Two 200-m-deep monitoring wells at the middle of the BHE field and a 300-m-deep monitoring well at the lower side of the BHE field was used to take core samples for measuring rock properties, and to measure the in-situ geothermal gradient and hydraulic conductivity, as well as monitor the temperature and pressure of the groundwater. The characteristics of the BHE, heat pump, and rock are summarized in Table 2.2.

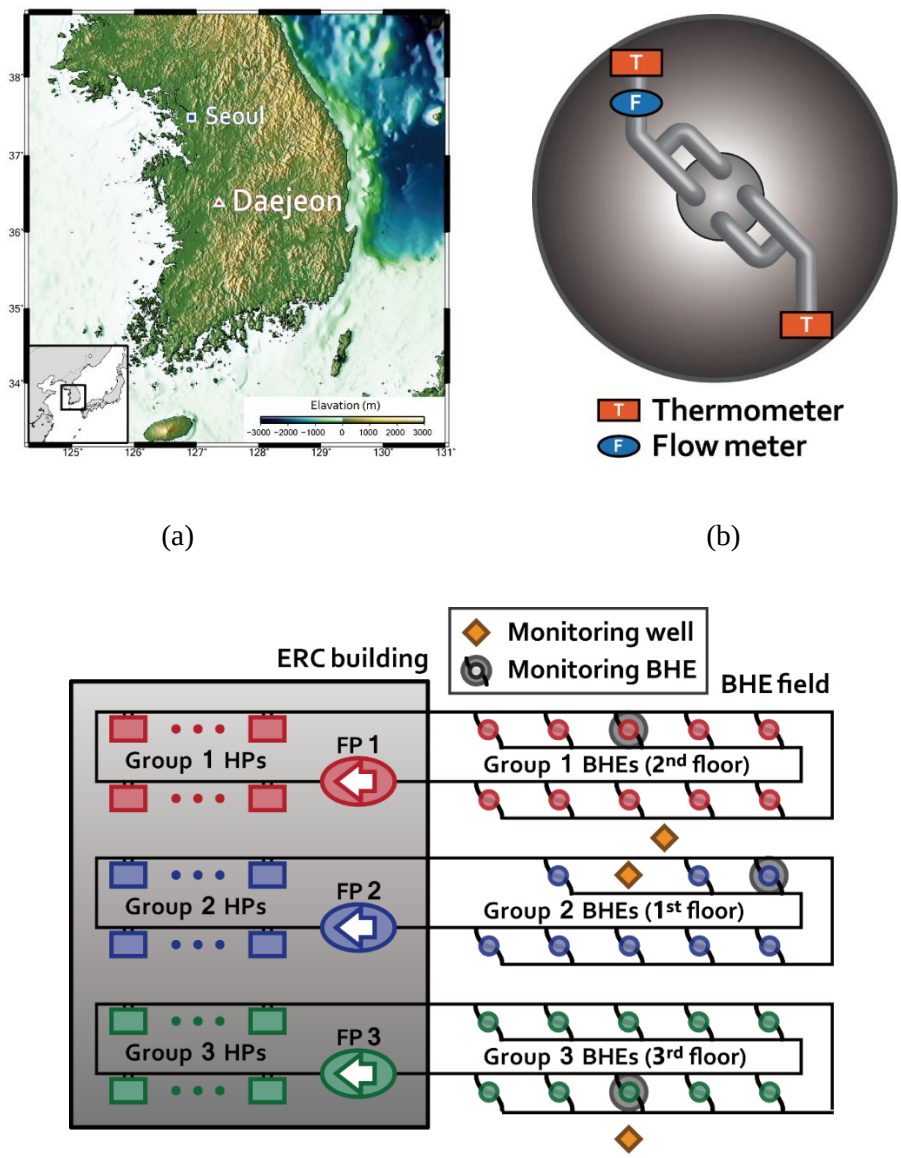


(a) (b)

(c)

**Figure 3.7.** Study area: (a) the map of the study area, (b) schematic diagram of the monitoring BHE, (c) layout of the GHP and its monitoring system for the ERC building.

### 3.4.2. Model setup

The new grid generator can produce a simulation domain with 28 BHEs in the KIGAM GHP system. The domain dimensions are set as 200 m in both horizontal directions and 320 m in the vertical direction from the ground surface, which are sufficiently large to avoid boundary effects (Figure 3.8a). Figure 3.8b illustrates an IFD grid at the periphery of the BHE with a double U-tube. Boundary conditions for the simulation are the same as those used in the previous chapter listed in Table 2.3. EOS3 for water and air is used in this model. The diurnal and interseasonal variations of the ground surface temperature and the unsaturated zone near the ground surface are ignored in the simulation, for the same reasons in Chapter 2.

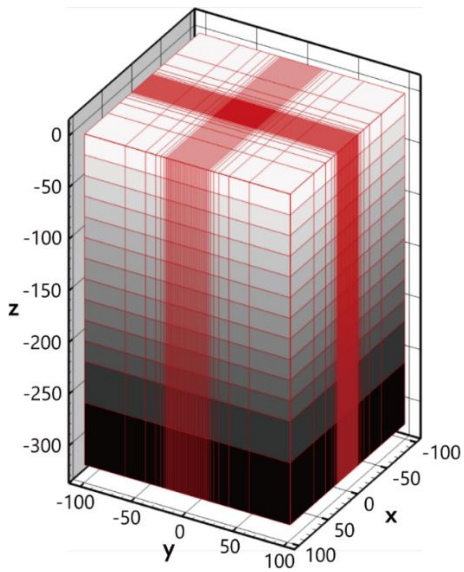


(a)

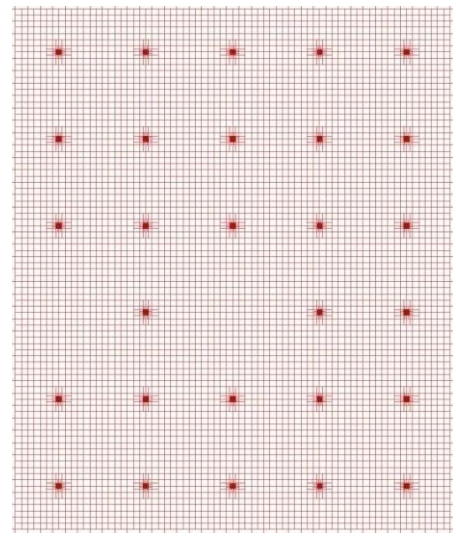

(b)

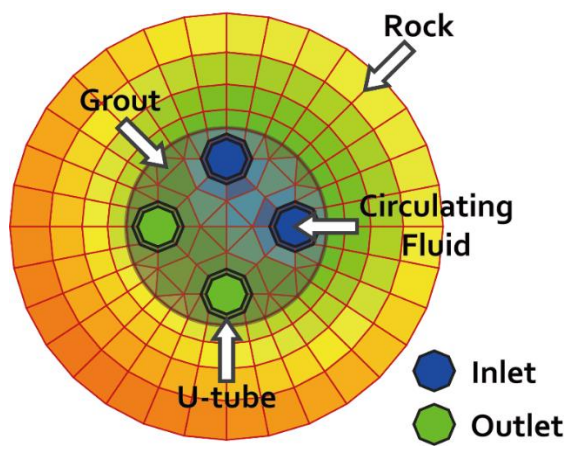


(c)

**Figure 3.8.** IFD grid: (a) complete model domain, (b) plan view of the domain, and (c) plan view at the periphery of the BHE.

### 3.4.3. Guidelines

To evaluate the long-term performance of the KIGAM GHP system, a simulation of the 25-year operation of the system is accomplished by injecting heat/cold to the ground through BHEs. The injection rate of the heat/cold is estimated by considering the hypothetical operation pattern obtained in accordance with the calculating method specified in Annex 4, Korean Agency for Technology and Standards 9306, 1999. Figure 3.9 illustrates the operation pattern of the system. The system is only operated for 12 hours per day over 5 days per week during the cooling/heating seasons. The starting value of the *OR* is set to 0.6 and it will be automatically controlled to hold the $p_{HP\text{-}indoor}$ constant. With the *OR*, assumed $T_{indoor}$, and initial $T_{avr}$, the $p_{HP\text{-}indoor}$ is calculated only once at the first time step of the cooling/heating simulations, respectively. The $T_{indoor}$ is assumed to be 28℃ during the cooling season and 18℃ during the heating season, which are the indoor temperatures recommended for Korean public institutions by the Korean government. The calculated $p_{HP\text{-}indoor}$ is listed in Table 3.2.

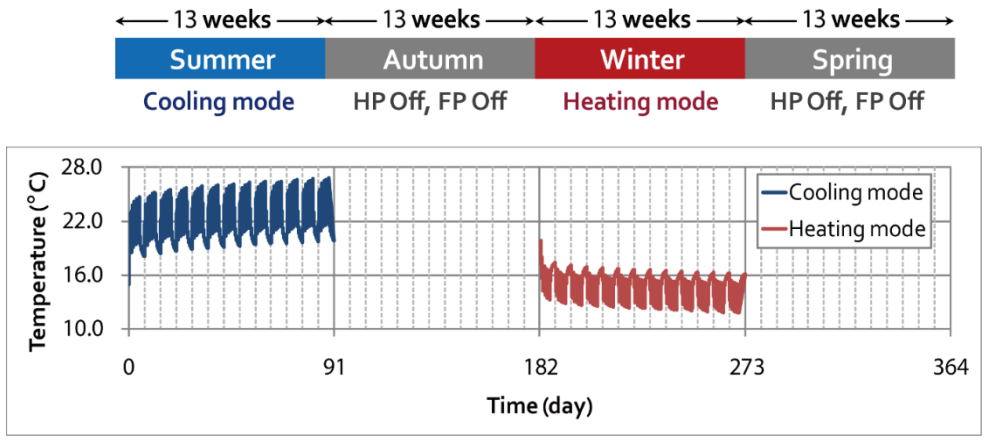


(a)

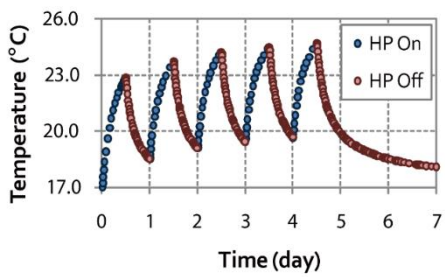


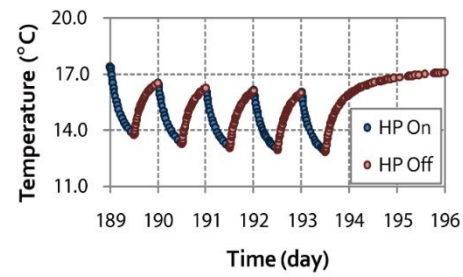


(b) (c)

**Figure 3.9.** Operation patterns of the system: (a) annual operation pattern, (b) weekly operation pattern for the cooling season, and (c) weekly operation pattern for the heating season. The $T_{avr}$ is influenced by the operation patterns.

**Table 3.2.** Calculated $p_{HP\text{-}indoor}$ of heat pumps on each floor for the cooling and heating seasons.

| | **Cooling season** | **Heating season** |
|---|---|---|
| **1F** | 89 kW | 107 kW |
| **2F** | 94 kW | 123 kW |
| **3F** | 100 kW | 131 kW |

### 3.4.4. Results and discussion

Figure 3.10 shows temperature fields after the cooling/heating seasons of the second operating year, 10th operating year, and 25th operating year, respectively. The temperature of the ground in the vicinity of BHEs is gradually increased with time because the *OR* and $p_{HP\text{-}CF}$ injected to the ground during the cooling season is higher than the *OR* and $p_{HP\text{-}CF}$ extracted from the ground during the heating season (Figure 3.11) and the ground is not fully recovered thermally during the off-season. As a result of increasing the temperature of the ground, Figure 3.11a shows that the $T_{avr}$ is also increased during the cooling/heating seasons. The reasons that the $T_{avr}$ and its increasing rate of the first floor (group 2 in Figure 3.7) is the highest during the cooling season seem to be that the location of the group 2 BHEs is at the middle of the BHE field, as well as that the number of the group 2 BHEs is less than the number of BHEs in the other groups. The $T_{avr}$ and its increasing rate of the first floor during the heating season, on the other hand, is not the highest. It would seem to be that the increased temperature of the ground has a positive effect on the performance of the group 2 BHEs. The $p_{HP\text{-}CF}$ is slightly increased with time (Figure 3.11b), in contrast, the *OR* is definitely changed with time (Figure 3.11c). Figure 3.12 shows the $p_{electric}$ and the $COP_C$/$COP_H$ with time during the cooling/heating seasons. During the cooling season, the $p_{electric}$ is increased and $COP_C$ is decreased with time rapidly. During the heating season, the opposite results are shown. The reason of the

particularly high $COP_C/COP_H$ of the first floor is that the efficiency of the group 2 heat pumps is better than the efficiency of the other group's heat pumps.

The performance of the KIGAM GHP system can be decreased if this imbalanced operation pattern is continued for long periods. Although the operation pattern used in the simulation is hypothetical, Figure 3.13 shows the actual increase of the groundwater temperature measured at two different depth in the 300-m-deep monitoring well for about two years. These data, of course, cannot be evidence for increasing the ground temperature induced by operating the GHP system, because the monitoring period is too short. The actual operation pattern cannot, in addition, be identical to the hypothetical operation pattern. However, in the case that the continuous increase/decrease of the ground temperature is observed from the long-term monitoring, the effort for balancing the both injected and extracted thermal powers, considering the thermal recovery of the ground, should be followed.

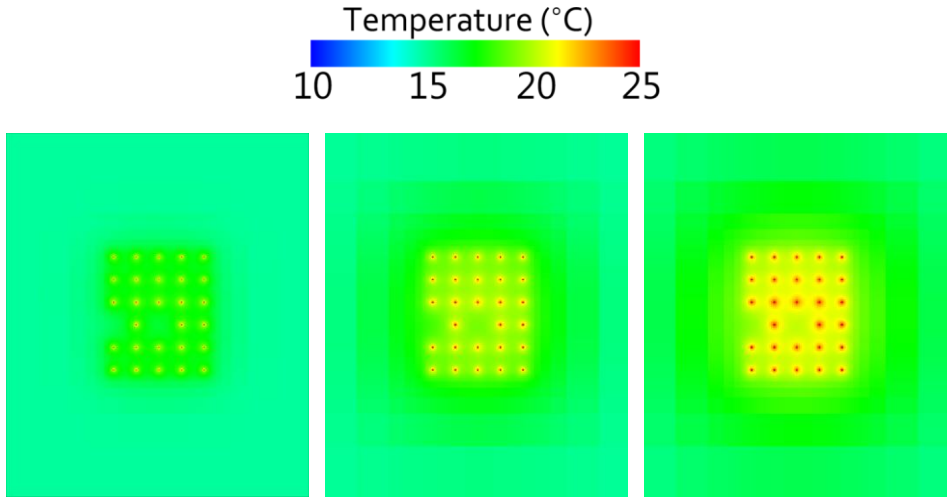


(a)

(b)

**Figure 3.10.** Temperature field of the second operating year (left), 10th operating year (middle), and 25th operating year (right): (a) after the cooling season and (b) after the heating season.

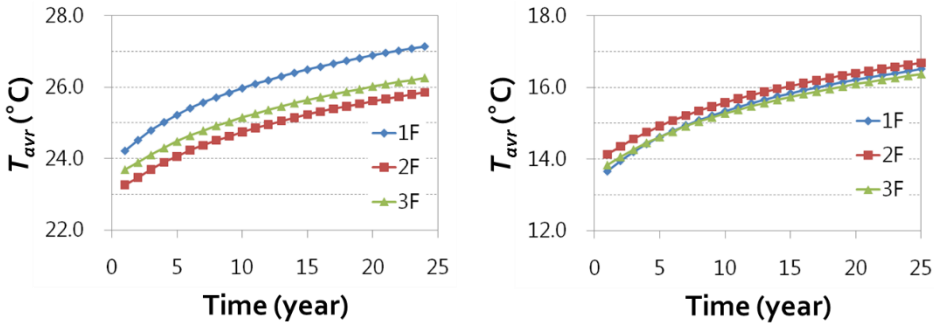


(a)

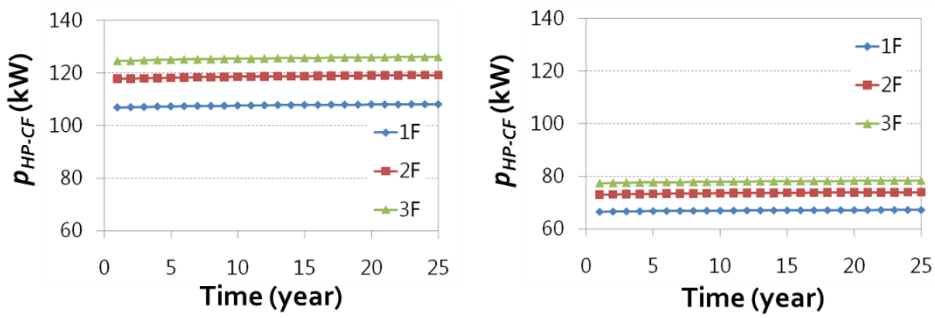


(b)

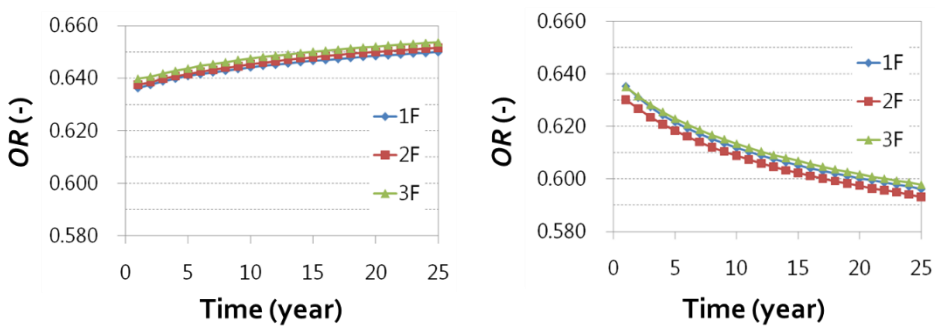


(c)

**Figure 3.11.** Changes of the (a) $T_{avr}$, (b) $p_{HP\text{-}CF}$, and (c) *OR* with time during the cooling (left) and heating (right) seasons.

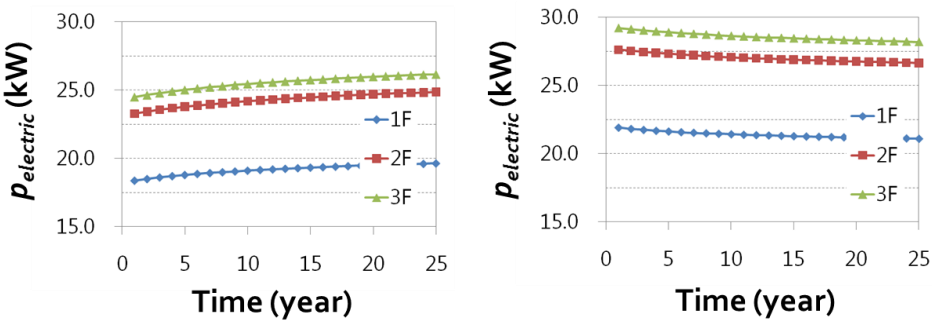


(a)

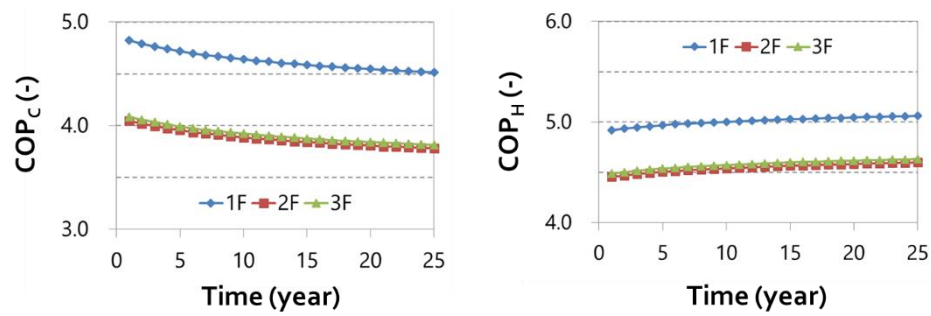


(b)

**Figure 3.12.** Changes of the (a) $p_{electric}$, and (b) $COP_C$/$COP_H$ with time during the cooling (left) and heating (right) seasons.

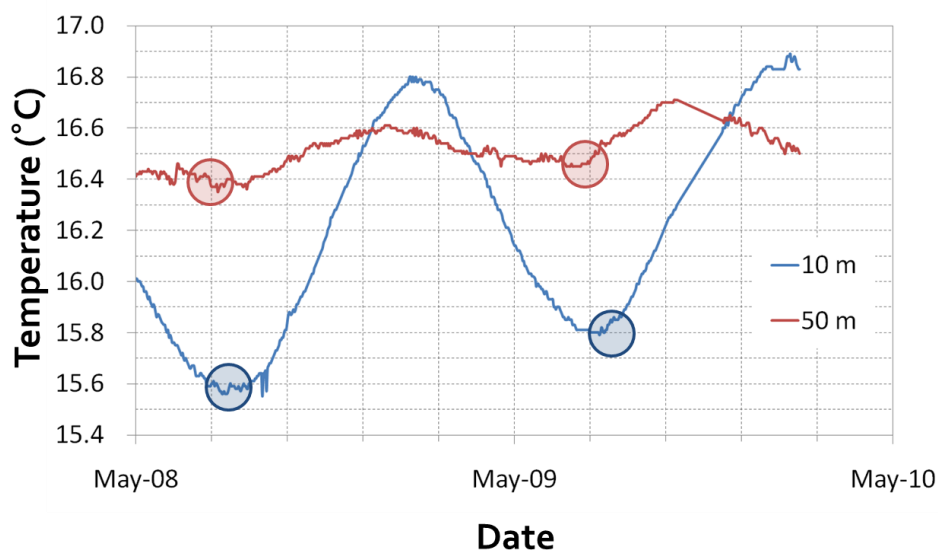


**Figure 3.13.** Groundwater temperature measured at two different depths in the 300-m-deep monitoring well for about two years.

## 3.5. Summary and conclusion

The new simulation model for multiple BHEs, which is based on the TOUGH2-MP, a massively parallel version of the TOUGH2 code, was developed for improving distributing memory requirements and computational efficiency. The parallel simulation code showed almost identical performance to the ideal linear speedup. It can consider thermal interactions between BHEs when the system is in operation and thermal storage in the ground after the operation period of the system so that it can be applied to evaluate the performance of the KIGAM GHP system for a 25-year operation.

The temperature of the ground in the vicinity of BHEs was gradually increased with time because of the imbalance of the injected/extracted thermal power to/$_{\text{from}}$ the ground during the cooling/heating season. It can cause the decrease of the $COP_C$, an efficiency of the system during the cooling season, for the long-term operation. If the continuous increase/decrease of the ground temperature is observed from the monitoring, the effort for balancing the injected/extracted thermal power should be followed.

The developed simulation model can be re-applied to the sensitivity analysis on parameters of the BHE design and the evaluation or optimization of the BHE design, considering with effects of the thermal interactions and thermal storage.

Then, it is expected that more practical and accurate results can be obtained than the previously studied results.

# Chapter 4. Improving accuracy and flexibility of numerical simulation of geothermal heat pump systems using Voronoi grid refinement approach

## 4.1. Introduction

Geothermal heat pump (GHP) systems use low-enthalpy geothermal energy resources for heating and cooling purposes. Several types of GHP systems such as closed-loop systems, open-loop systems, and standing column well systems, commonly consist of heat pumps, fluid pumps, and geothermal wells. The geothermal wells, except for the open-loop system, contain pipes for exchanging heat between the fluid inside the pipe and ground or groundwater outside the pipe. The schematics of typical GHP systems and geothermal wells of them are shown in Figure 4.1.

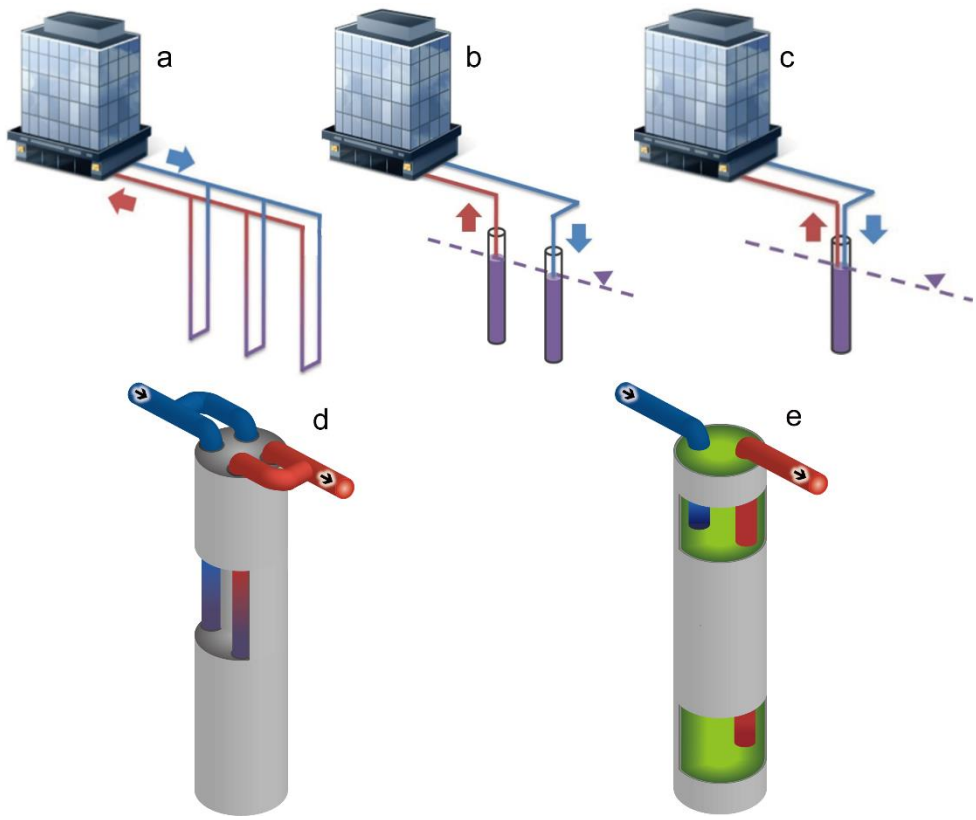


**Figure 4.1.** Types of the geothermal heat pump system: (a) vertical closed-loop system, (b) open-loop system, and (c) standing column well system; geothermal wells: (d) borehole heat exchanger of the vertical closed-loop system and (e) bi-axial standing column well. Cold water from heat pumps is injected into the ground and then warm water heated by ground is produced for heating operation.

TOUGH2 (Pruess et al., 1999) is a widely used numerical simulator for geothermal reservoir engineering (Pruess, 2004). It can be also applicable to GHP systems with some modifications (Kim et al., 2010). Like all simulations, a well-designed grid is required for minimizing numerical errors and then maintaining the desired level of accuracy in simulations of the GHP systems. Areas of particular interest in the geothermal field are the inside and surrounding of geothermal wells in which dramatic shifts of pressure and temperature are occurred. The accuracy of the numerical formulation can be improved by increasing grid resolution in those areas.

The general form of the basic mass and energy balance equations of TOUGH2 is

$$\frac{d}{dt}\int_{V_n} M dV_n = \int_{\Gamma_n} \mathbf{F}\cdot\mathbf{n}\, d\Gamma_n + \int_{V_n} q dV_n, \tag{4.1}$$

where $V_n$ denotes a subdomain bounded by the closed surface $\Gamma_n$ and **n** is a normal vector on surface element $d\Gamma_n$, pointing toward $V_n$. The quantity $M$ denotes mass or energy per volume. **F** represents mass or heat flux and $q$ represents sources or sinks. In all codes of the TOUGH family such as TOUGH2, TOUGHREACT (Xu et al., 2011), and TOUGH2-MP (Zhang et al., 2008), the continuum equation (4.1) is discretized in space using an integrated finite difference method (IFD; Edwards, 1972; Narasimhan and Witherspoon, 1976), often referred to as a finite volume method. The discretized equations are valid for arbitrary irregular discretizations in multi dimensions (Pruess et al., 1999). This discretization flexibility should be used carefully, however, because the accuracy of solutions depends upon an angle ($\theta$ in

Figure 4.2) between the connection interface and the line joining the centers of two grid blocks. The accuracy of the IFD formulation is reduced if the $\theta$ is not 90˚, because flux **F** is defined to be normal to the $d\Gamma_n$ in equation (4.1).

TOUGH2 offers a grid generation module, MESHMaker, which can generate both 2-D radially symmetric grids and 3-D rectangular Cartesian grids. The rectangular Cartesian grids generated by MESHMaker is identical to the typical finite difference (FD) grids that always satisfy that $\theta = 90$˚. The FD is, however, not an efficient method for local grid refinement, because if local grid refinement is carried out in the regions of interest, then the whole domain is influenced by it and unnecessary grid blocks located far away from the regions of interest can be generated. On the other hand, conventional triangular meshes used in finite element method are suitable for local refinement, but they cannot satisfy the orthogonal condition of IFD formulations.

Several TOUGH2 meshing programs such as WinGridder (Pan, 2003), PetraSim (Alcott et al, 2006), TOUGH2GIS (Berry et al., 2014), MeshVoro (Freeman et al., 2014), and AMESH (Haukwa, 1998) have been developed. They have commonly adopted Voronoi tessellations (Voronoi, 1908) to generate TOUGH2 grids. The Voronoi grid always meets the orthogonal condition. Thus it is suitable for local refinement of the TOUGH2 grid. Since these programs are made for general geothermal reservoir simulations using TOUGH2, they cannot generate unstructured grids that include detailed shapes of the cross-sections of wells and pipes inside the wells (Figure 4.1d and e).

In our previous study (Kim et al., 2010), we developed the grid generator for borehole heat exchangers (BHEs) that is a component of vertical closed-loop geothermal heat pump systems (Figure 4.1a and d). It was validated by datasets from the thermal response test and actual operations and applied to evaluate design of BHEs without remarkable errors, although the grid generated from it did not satisfy the orthogonal condition.

This paper presents the method developed for generating unstructured grids particularly for the geothermal heat pump systems and its implementation with a computational algorithm composed of a series of newly developed or existing codes. This method adopts the Voronoi tessellation for generating the grid so that the orthogonal condition is always satisfied. It can include detailed shapes of the cross-sections of the geothermal wells within the unstructured Voronoi grid. Thus, it can generate the grids for the open-loop and standing column well (SCW) systems, as well as for the vertical closed-loop systems. The generated grid and TOUGH2 simulation results using it can visualize with ParaView, which is a powerful open source application for scientific visualization.

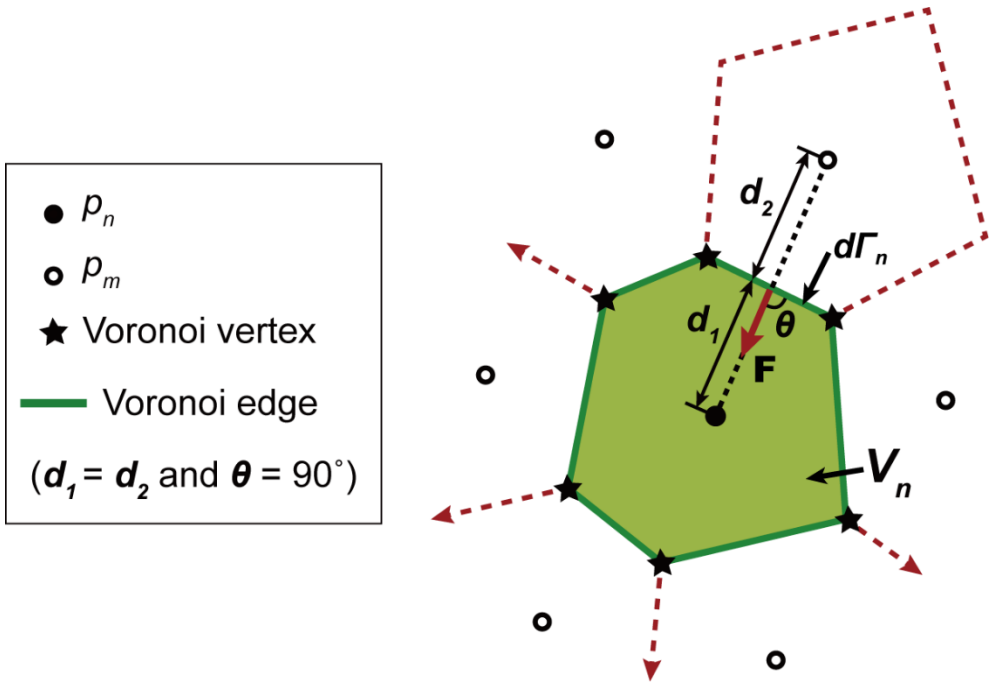


**Figure 4.2.** Space discretization and geometric parameters in the integrated finite difference method and Voronoi diagram. The connections between two adjacent cells are always orthogonal to their connection interface (Voronoi edge). The flux **F** is also defined to be normal to the connection interface $d\Gamma_n$. In the integrated finite difference method, contrary to Voronoi diagram, the condition of $d_1 = d_2$ is not necessary.

## 4.2. Method

The Voronoi cell $\{V_n\}$ in Figure 4.2 can be defined as

$$\{V_n\} = \{p: \| p - p_n \| < \| p - p_m \|, \forall m \neq n\}. \quad (4.2)$$

This equation means that a set of given points $p$, called seeds or Voronoi seeds, in the domain has a non-overlapping territory $\{V_n\}$ that is the area of the plane closer to that point $p_n$ than to any other point $p_m$. Then, the common boundary of two Voronoi cells, called a Voronoi edge, passes the center of two neighboring seeds and is perpendicular to the lines joining the two seeds. Intersections of Voronoi edges are called Voronoi vertices that are the nodes equidistant to three (or more) seeds. Two mathematicians, Dirichlet (1850) and Voronoi (1908), were the first to introduce this concept (Green and Sibson, 1978; Weatherill, 1988; Aurenhammer and Klein, 2000). A Voronoi tessellation, a Voronoi diagram, or a Voronoi decomposition was named after him. Therefore, the connections between two adjacent grid blocks in a Voronoi grid are always orthogonal to their connection interface.

To construct unstructured Voronoi grids that include shapes of the cross-section of wells or pipes, the seeds relevant to wells or pipes should lie on specific positions. For example, a circular-shaped polygon (*Py* in Figure 4.3a) bounded by Voronoi edges can be easily obtained with two sets of concyclic seeds, which lie on two concentric circles ($C_1$ and $C_2$ in Figure 4.3a). The *Py* is a convex polygon that circumscribes the circle that is also concentric with and equidistant from the $C_1$ and

$C_2$. A pair of seeds ($p_1$ and $p_2$ in Figure 4.3a) on the $C_1$ and $C_2$ has to be placed on the line ($L_{12}$ in Figure 4.3a) perpendicular to the corresponding edge of the *Py*. Two neighboring pairs of seeds (seeds of four adjacent grid blocks) are vertices of the virtual isosceles trapezoid (*Trap* in Figure 4.3a), and consequently share one Voronoi vertex (*vtx* in Figure 4.3a).

The smoothness of the curvature (how similar the *Py* is with the circle) depends on the uniformity of the distribution and the number of seeds that lie on the concentric circle. The seeds do not have to lie uniformly on the circle (Figure 4.3b), although the *Py* is less similar to the circle as the seeds lie more non-uniformly on the circle. They have only to be placed on the intersections of the concentric circles and the $L_{12}$. The *Py* is still a convex polygon that circumscribes the circle to be formed. This is a helpful feature for generating the unstructured grid that includes detailed shapes of the cross-section of wells and pipes inside the wells, because it increases the degrees of freedom of the grid. As the number of seeds on the circle is more, of course, the *Py* is the more similar with the circle. As the number of grid blocks is more, however, the calculation time is longer. On the contrary, the shape of the *Py* can be changed unintendedly by intruded seeds, where the intruded seeds are closer to the area between the seeds that lie on the circle, which is supposed to be closer the seeds that lie on the circle than any other seeds. Therefore, the number of seeds on the circle should be determined carefully to consider the tradeoff between accuracy and efficiency.

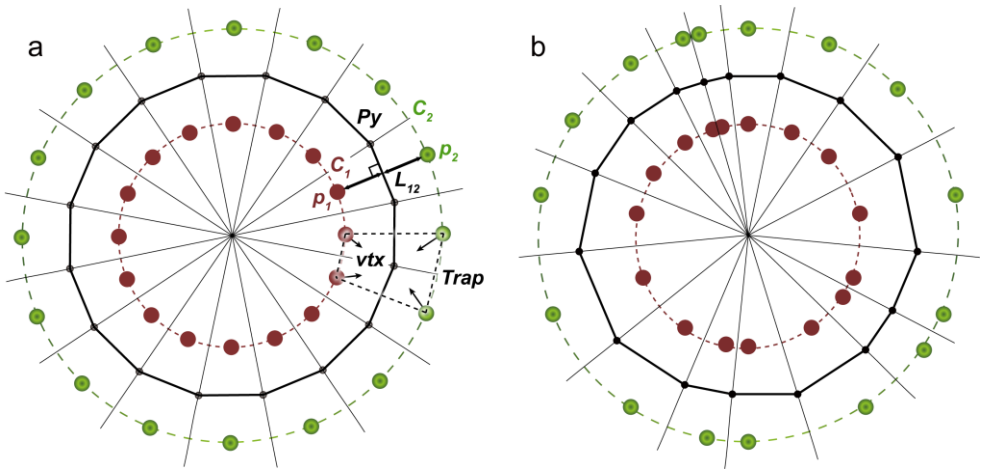


**Figure 4.3.** Circular-shaped polygons (*Py*) bounded by Voronoi edges obtained with two sets of concyclic seeds, which lie on two concentric circles ($C_1$ and $C_2$): (a) Circular-shaped polygons with seeds lain uniformly on the circle and (b) seeds lain nonuniformly on the circle.

Using this method, a code that can generate seeds needed for constructing a 2-D unstructured Voronoi grid that takes the location, configurations, and dimensions of the wells and pipes in a geothermal field into account is developed. The developed code, called Voronoi seeds generator (VSG), generates seeds categorized into three types of layers: rectangular, circular, and well layers. The rectangular layer is a set of seeds that are vertices of small rectangles into which a large rectangle is partitioned. The dimensions and numbers of the small rectangles can be set to the desired values. The circular layer is a set of seeds that lie uniformly on concentric circles. The radiuses of circles and the number of seeds can be set to the desired values. The well layer is a set of seeds, which contains the geometry of the cross-section of geothermal wells. The coordinates of the center and dimensions of the layer can be set to the desired values. The layers can be overlapped with each other for local refinement. In the overlapped area, the seeds on the subjacent layer are deleted.

MATLAB is used for checking of the generated seeds, which can compute and plot Voronoi diagrams for the seeds "x,y" through the "voronoi(x,y)" function (Persson and Strang, 2004). Checking the position and density of the generated seeds with the plot can reduce truncation errors and give better results.

To construct the Voronoi grid from the seeds generated by VSG, coordinates of the Voronoi vertices should be calculated. MATLAB can, as mentioned above, compute Voronoi diagrams. Automatic connections of it to VSG or other codes through script files, however, seemed to be difficult, since it is not an

open-source program. Fortune (1987) devised an algorithm, called Fortune's algorithm, which is the most popular way of computing Voronoi grids. Several open-source codes or programs have been developed to implement the Fortune's algorithm. In this study, AMESH is used to calculate the Voronoi vertices. Accordingly, VSG produces two outputs: input files for AMESH and MATLAB, respectively. AMESH is originally developed to generate 1-D, 2-D, or 3-D (horizontal projections of the 2-D areal plane) grids of TOUGH2 from the list of locations of grid blocks. Therefore, not only connections of it to the outputs of VSG is simple, but also generation of the 3-D grid and TOUGH2 input files from the outputs of it can be easy.

The next step is to generate the 3-D grid and TOUGH2 input files from the 2-D outputs of AMESH. A series of codes are developed: 1) to collect the coordinates of the nodes (Voronoi vertices) and the connection information of the elements (grid blocks) from the output files of AMESH, 2) to compute the global node number by using the local node number, element number, and coordinates of the nodes, which is not provided from the outputs of AMESH, but the essential information required to visualize the grid, 3) to generate the 3-D grid and TOUGH2 input files, which contain 3-D geometries and properties of wells, pipes and geological features, 4) to extract the pressure and temperature data from the output file of TOUGH2, and 5) to visualize the generated 3-D grids and TOUGH2 simulation results with ParaView. Figure 4.4 represents the flow chart of the computational algorithm for implementing the developed method.

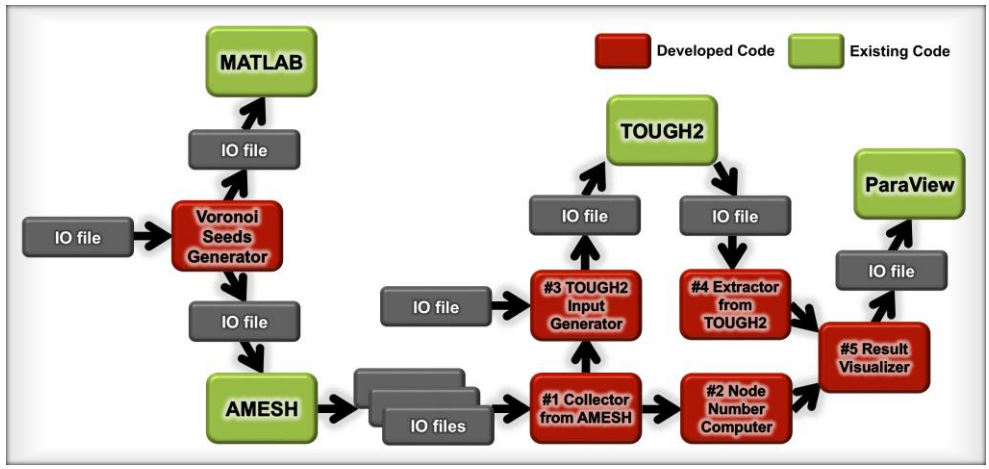


**Figure 4.4.** A flow chart of the computational algorithm for implementing the developed method. Some of codes are newly developed in this study (red) and others already exist (lime).

## 4.3. Results

### 4.3.1. Examples of generated grids

The generated grids visualized with ParaView shown in Figure 4.5 represent BHEs in vertical closed-loop systems. Figure 4.6 shows the generated grid for the open-loop and SCW systems. In both horizontal and vertical directions, the number, location, and size of pipes inside the borehole can be adjusted by changing the properties in the input files of the developed codes. Figure 4.5d, 4.5e, 4.5f, 4.6d, 4.6e, and 4.6f show results of changing these properties of pipes in the horizontal direction. The material properties of the grid blocks can also be adjusted. The different colors in Figure 4.5 and 4.6 represent different materials which are the fluid inside the pipe (dark brown), the pipe wall (red), the grout (pink), the groundwater inside the well (lime), and the ground (ivory). The number of grid blocks corresponding to the fluid or groundwater is just one in horizontal direction because TOUGH2 cannot calculate the turbulent flow in pipes or wells, but can only consider laminar flow in porous media described by Darcy's law. Therefore, the pressure and temperature of the fluid in pipes or groundwater in wells are only allowed to vary along the z-direction. On the contrary, the grid corresponding to the grout and pipe of the closed-loop system is split into many grid blocks for calculating the conduction of heat.

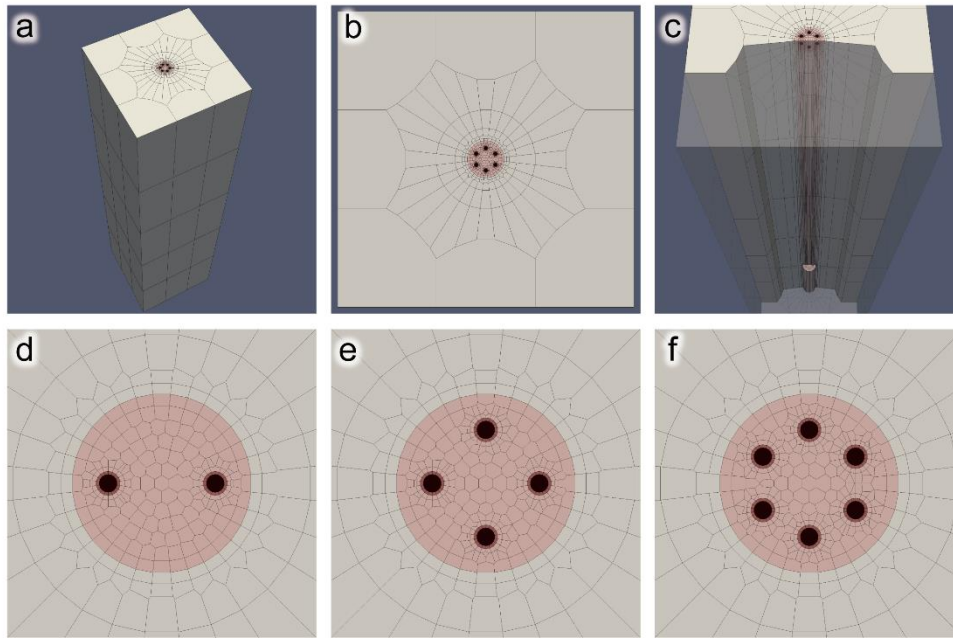


**Figure 4.5.** Generated grids for vertical closed-loop systems: (a) whole 3-D grid, (b) plan view, (c) translucent view, (d) single U-tube BHE, (e) double U-tube BHE, and (f) triple U-tube BHE.

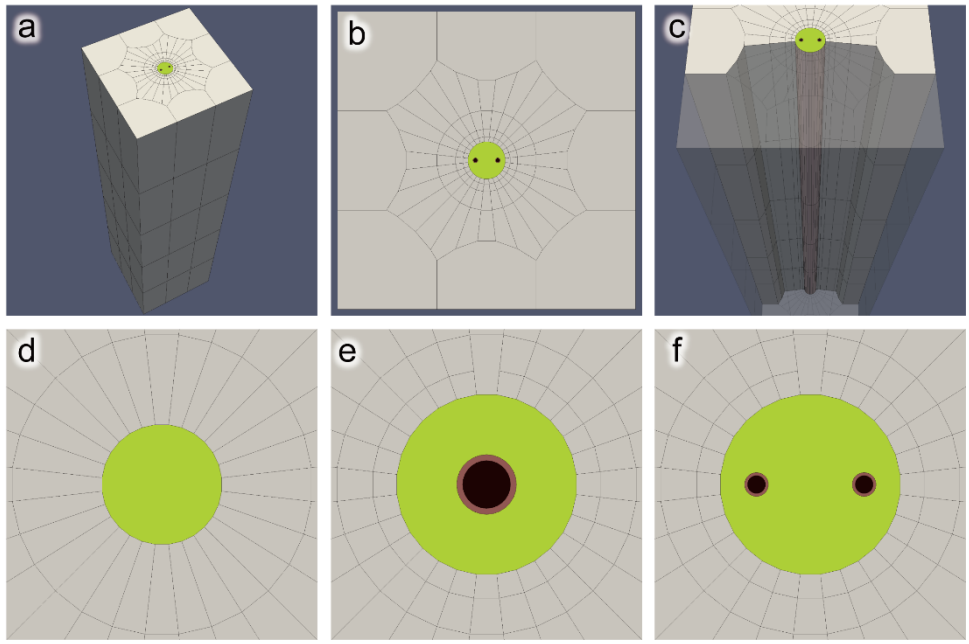


**Figure 4.6.** Generated grids for the open-loop and SCW systems: (a) whole 3-D grid, (b) plan view, (c) translucent view, (d) open-type well, (e) co-axial SCW, and (f) bi-axial SCW.

The 3-D grid is generated by extending the first planar (2-D) grid in the vertical direction. In the first planar grid (the first layer of the 3-D grid), all wells and pipes are placed at their positions. As the layer increases in depth, the layer depth can be deeper than the length of certain wells or pipes. Then, the geometries and material properties of the grid are changed according to the remaining wells and pipes.

In the vertical closed-loop system, pipe pairs in the borehole are joined with a U-shaped cross connector at the bottom of the borehole. The length of the pipe in the vertical direction is much longer than the length of the cross connector in the horizontal direction. Hence, the grid generated for the real configuration can cause numerical instability due to the relative difference in the size of the two grid blocks. Fortunately, grid blocks located apart from each other can be connected in TOUGH2. Therefore, grid blocks corresponding to the vertical pipe pairs at the bottom are connected so that the fluid can circulate through the pipe without the numerical instability.

### 4.3.2. Example simulation

An example simulation to demonstrate the use of the developed method is performed with the generated grid shown in Figure 4.7, which includes four different kinds of geothermal systems. This simulation has not attempted to assess the mathematical integrity of the generated grid or to obtain the meaningful results from

this simulation. Thus, the simplified setting and representative materials are used for this simulation. Dimensions and properties of simulation parameters are listed in Table 4.1. Boundary, initial and source/sink conditions of the simulation are described in Table 4.2. Different injection and production rates, depending on the system, are used in the simulation to clarify the effect of the injection and production on the pressure and temperature changes. The injection water temperature (20℃) is higher than the ambient groundwater temperature (15℃). The warm water is injected to the injection pipe(s) or well of each system during 12 hours. Therefore, we can expect that the production water temperature is 15℃ at first and gradually increased up to 20℃ during the simulation.

TOUGH2-MP is used in this simulation and the simulation runs without any problems. The simulated pressure and temperature after 12 hours are shown in Figure 4.8. Pressure and temperature are both increased at the injection pipe(s) and well of each system, while pressure is decreased and temperature is slightly increased at the production pipe(s) and well of each system. Higher injection and production rates of the open-loop wells than those of other wells have more effect on the whole domain.

Temperature differences between production and injection pipe(s) or well of each system are definitely shown in Figure 4.9, because both the boundary and initial conditions of the temperature are assigned to be the same at 15℃. The temperature at the injection point almost equal to the injection temperature (20℃) and the temperature at the production point is higher than the initial temperature by

affecting the injection temperature. The temperature increase in the middle of the well, at which the exit end of the injection pipe is located, is shown in Figure 4.9b and c. The injected water flows out from the pipe and directly increases the surrounding temperature.

The pressure and temperature distributions shown in Figure 4.8 and 4.9 are not different from common expectations. Therefore, the results of the example simulation performed with the generated grid can validate that there are no serious problems in the generated grid at least. Additional validations of the generated grid, of course, are needed for realistic field-scale applications. Then, the generated grid can be applied to simulations of design optimization of the geothermal heat pump systems, decision of the optimal injection and production rate of the fluid and heat, and prediction of the performance changes of the system caused by climate or environmental changes, besides any other simulations related to groundwater flow and heat transfer in the geologic media with boreholes.

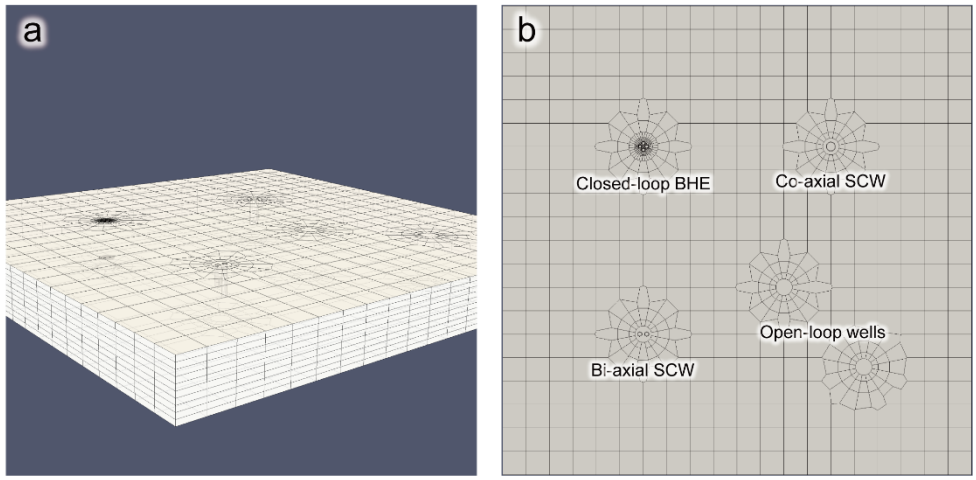


**Figure 4.7.** Generated grid for the example simulation including four different kinds of geothermal systems: (a) whole 3-D model domain (z-axis is downscaled to 1/500th) and (b) plan view of the grid with the well names.

**Table 4.1.** A summary of dimensions and properties of the model domain, wells, pipes, and materials used in the simulation

| | | | | | | |
|---|---|---|---|---|---|---|
| **Domain** | Dimensions | 10 m (0.5 m × 20 cells) in the x and y directions<br>500 m (50 m × 10 cells) in the z direction | | | | |
| **Well** | Diameter and length | 0.35 m, 400 m | | | | |
| **Pipe** | Diameter (outer), wall-thickness, and length | Closed-loop well: 0.07 m, 0.007 m, 400 m<br>Co-axial SCW: 0.2 m, 0.01 m, 300 m<br>Bi-axial SCW: 0.1 m, 0.01 m, 300/200 m (production/injection) | | | | |
| | | Density | Porosity | Permeability | Thermal conductivity | Specific heat |
| | | ($kg/m^3$) | (-) | ($m^2$) | (W/m-K) | (J/kgK) |
| **Material** | Ground | $2.60\times10^3$ | 0.1 | $1.13\times10^{-10}$ | 3.00 | $0.8\times10^3$ |
| | Fluids | $0.99\times10^3$ | 1.0 | $1.13\times10^{-7}$ | 0.58 | $4.2\times10^3$ |
| | Pipe | $0.92\times10^3$ | 0.0 | 0.0 | 0.37 | $2.0\times10^3$ |
| | Grout | $2.00\times10^3$ | 0.0 | 0.0 | 0.80 | $2.2\times10^3$ |

**Table 4.2.** A summary of boundary, initial and source/sink conditions of the simulation

| | | |
|---|---|---|
| **Boundary** | **Hydraulic** | No flow: top, bottom<br>Constant head: left, right, front, back |
| | **Thermal** | No flow: top, bottom<br>Constant temperature: left, right, front, back |
| **Initial** | **Hydraulic** | Hydrostatic pressure |
| | **Thermal** | Constant temperature (15℃) |
| **Source/Sink** | **Closed-loop well** | injection (0.1 kg/sec, 20℃, at two pipes) |
| | **Co-axial SCW** | injection (0.2 kg/sec, 20℃, at pipe)<br>production (0.2 kg/sec, at well) |
| | **Bi-axial SCW** | injection (0.2 kg/sec, 20℃, at 200 m pipe)<br>production (0.2 kg/sec, at 300 m pipe) |
| | **Open-loop wells** | injection (20 kg/sec, 20℃, at injection well)<br>production (20 kg/sec, at production well) |

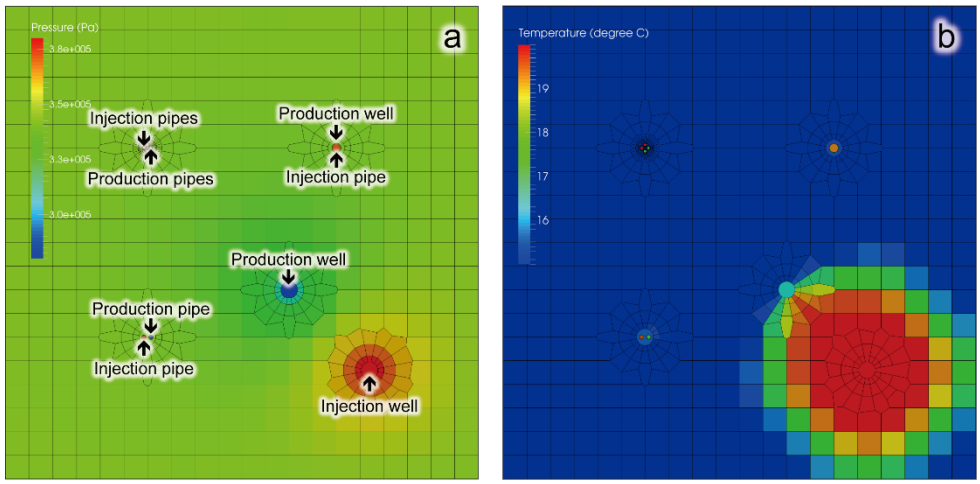


**Figure 4.8.** Pressure and temperature field on the surface after 12 hours: (a) pressure and (b) temperature.

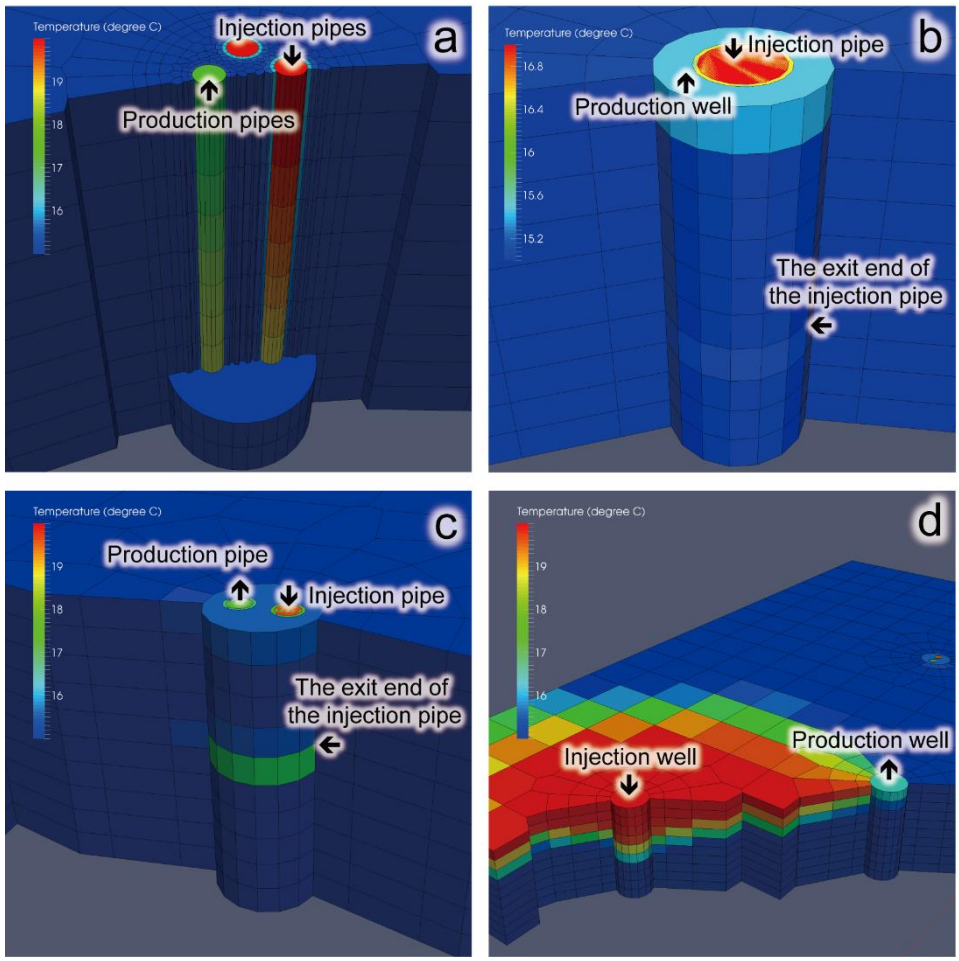


**Figure 4.9.** Temperature at the periphery of the wells: (a) closed-loop system, (b) co-axial SCW system, (c) bi-axial SCW system, and (d) open-loop system.

## 4.4. Conclusion

The presented method for generating the specific-shaped Voronoi grid is successfully applied to the grid refinement in and around geothermal wells. The computational algorithm composed of a series of newly developed or existing codes generates well- and pipe-shaped Voronoi grid in addition to satisfying the orthogonal condition of the IFD formulation. The visualization of the generated grids are accomplished by ParaView and the detailed shape of the geothermal wells are clearly seen in the grid. The generated grid is demonstrated with the simple simulation example of water production/injection from/to the various kinds of the geothermal wells. Simulation results show that distributions of pressure and temperature seem to be acceptable for use the generated grid in evaluations of the geothermal heat pump systems. The product of this work can be utilized at the most of simulations using TOUGH2. Geothermal heat pump simulations which are needed where smaller-scale details of the model behavior should be resolved in and around the geothermal wells are the best targets of the developed method.

Although the computational accuracy and efficiency of the Voronoi grid itself have been tested by previous researches (Palagi and Aziz, 1994; Verma and Aziz, 1996; Croucher and O'Sullivan, 2013), there are still possible approaches to improve the accuracy and efficiency of it, such as approximating the seeds to the centroids of the cells (Du et al., 1999) and eliminating cells with very small faces

(Sieger et al., 2010). The code used to generate Voronoi faces and vertices from the seeds can handle a semi-3-D grid which is the horizontal 2-D grid with layers, rather than a fully 3-D grid. Typically the semi-3-D grids are enough to simulate physical processes occurred in the geologic media that has usually layered structure, but sometimes they are not. Developments of methods for generating fully 3-D grids with those approaches will be accomplished in the future studies, as well as validations and applications of the generated grid.

# Chapter 5. Discussion

In this thesis, to evaluate the design and performance of geothermal heat pump systems, the numerical simulator and grid generator are developed, upgraded and applied to several studies, such as the sensitivity analysis, design evaluation of the KIGAM GHP system, and long-term performance evaluation of the KIGAM GHP system. In this chapter, their meanings, limitations, and new directions for future studies are discussed.

The sensitivity analysis of design parameters that can affect the performance of the BHE is performed by utilizing the advantages of the 3-D numerical simulator that can consider most design parameters and grid generator that includes the detailed shape of the cross-section of the BHE. Simple analytical solutions can not consider some parameters, e.g. groundwater flow and heat transfer coefficient. Now, the latest versions of the numerical simulator and grid generator can consider more design parameters such as the spacing between BHEs and the SCW and open-loop systems than the previous ones. The sensitivities of such parameters on the performance and costs of various GHP systems can be analyzed in the future studies.

The design of BHEs for use of low-enthalpy geothermal energy is evaluated in field-scale demonstrations, the KIGAM GHP system, by considering the installation and operation costs of the system. This can be possible only if the

variation of the electric power supplied to operate the heat pump with the temperature of the circulating fluid and indoor is calculated. The limitation of this study is that the effects of thermal interactions and thermal storage are not considered because only one BHE can be included in the simulation model at this time. In the future study, I think that the more meaningful results can be achieved through simulating the GHP system using the lasted version of the simulation model.

The long-term performance of the KIGAM GHP system is evaluated by the second version of the simulation version, so that the effects of thermal interactions and thermal storage can be considered. This study will be improved by adding various simulation cases related to the operation pattern, room temperature, and climate change. The groundwater temperature monitored at the KIGAM GHP system can be used effectively.

The latest version of the grid generator has the flexibility of including detailed shapes of the cross-sections of pipes at any position inside the geothermal wells, and mathematical integrity satisfying the orthogonal condition of the TOUGH2 grid, which is that connections between two adjacent grid blocks in a TOUGH2 grid should be orthogonal to their connection interface. The latest versions of the numerical simulator and grid generator have not been used in applications yet. They can be utilized at the most of TOUGH2 simulations related to groundwater flow and heat transfer in the geologic media with boreholes, as well as the geothermal heat pump simulations. Although the computational accuracy and efficiency of the Voronoi grid itself have been tested by previous researches, there

are still possible approaches to improve the accuracy and efficiency of it, such as approximating the seeds to the centroids of the cells and eliminating cells with very small faces. The code used to generate Voronoi faces and vertices from the seeds can handle a semi-3-D grid which is the horizontal 2-D grid with layers, rather than a fully 3-D grid. Typically the semi-3-D grids are enough to simulate physical processes occurred in the geologic media that has usually layered structure, but sometimes they are not. Developments of methods for generating fully 3-D grids with those approaches will be accomplished in the future studies, as well as validations and applications of the generated grid.

# Chapter 6. Summary and conclusions

In this thesis, a three-dimensional numerical simulation model is developed for optimizing the design and evaluating long-term performance of the GHP system. The vertical closed-loop GHP system is a main target of the study. Firstly, the simulation model that can estimate the performance of a vertical closed-loop GHP system was developed with based on the TOUGHREACT. It was validated by comparing two measurement datasets with their respective simulation results and applied in evaluating the KIGAM GHP system. The BHEs of the KIGAM GHP system seemed to be overdesigned unless electricity costs quadruple.

The upgraded model was developed to simulate the vertical closed-loop GHP system with multiple BHEs. For improving distributing memory requirements and computational efficiency, the base simulator of it is TOUGH2-MP into which the parallel computing algorithm is implemented. It can consider thermal interactions between BHEs and thermal storage in the ground by simulating multiple BHEs at once. It was applied to evaluate the long-term performance of the KIGAM GHP system for a 25-year operation. The imbalance of the injected/extracted thermal power to/from the ground during the cooling/heating season caused the decrease of the efficiency of the system during the cooling season for the long-term operation.
The grid generator was developed to produce well- and pipe-shaped grid in addition to satisfying the orthogonal condition of the IFD formulation. The grid generated

from it is tested by water production and injection simulations with the various kinds of the geothermal wells. It is not used in applications yet, but can be re-applied to the sensitivity analysis on parameters of the BHE design and the evaluation or optimization of the BHE design, considering with effects of the thermal interactions and thermal storage. Then, it is expected that more practical and accurate results can be obtained than the previously studied results. It can be applied to the new study for the open-loop and SCW GHP systems, as well as the vertical closed-loop GHP system. Which one of these systems is the best depends on the geothermal and hydro-geologic conditions of the ground, available land, and local installation costs at the site. Therefore, the ultimate goal of the future study will be to develop a simulation model that can provide the type of the best GHP system and the proper design and optimal operation method of the selected GHP system.

# References

Alcott, A., Swenson, D., and Hardeman, B. (2006) Using PetraSim to create, execute, and post-process TOUGH2 models. TOUGH Symposium 2006, Berkeley, California, May 15–17, p. 1–6.

Aurenhammer, F., and Klein, R. (2000) Voronoi diagrams. Handbook of computational geometry, 5, 201–290.

Bennett, C.O. and Meyers, J.O. (1982) Momentum, heat, and mass transfer, Third ed., Wiley, New York.

Berry, P., Bonduá, S., Bortolotti, V., Cormio, C., and Vasini, E.M. (2014) A GIS-based open source pre-processor for georesources numerical modeling. Environmental Modelling and Software, 62, 52–64.

Bird, R.B., Stewart, W.E., and Lightfoot, E.N. (1960) Transport Phenomena. Wiley, New York, 780 p.

Croucher A.E. and O'sullivan M.J. (2013) Approaches to local grid refinement in TOUGH2 models. 35th New Zealand Geothermal Workshop, Rotorua, Nov. 17–20, p. 1–7.

Diersch, H.-J.G. (2005) FEFLOW finite element subsurface flow and transport simulation system, Reference Manual, User's Manual and White Papers Vol. I, II, III, IV, WASY – Institute for Water Resources Planning and Systems Research, Berlin.

Dirichlet, L.G. (1850) Uber die Reduction der positiven quadratischen Formen mit

drei unbestimmten ganzen Zahlen. Journal für die Reine und Angewandte Mathematik, 40, 209–227

Dittus, F.W. and Boelter, L.M.K. (1930) Heat Transfer in Automobile Radiators of the Tubular Type. University of California Publications in Engineering, 2, 443–461.

Du, Q., Faber, V., and Gunzburger, M. (1999) Centroidal Voronoi tessellations: applications and algorithms. Society for Industrial and Applied Mathematics review, 41, 637–676.

Edwards, A.L. (1972) TRUMP: A Computer Program for Transient and Steady State Temperature Distributions in Multidimensional Systems, National Technical Information Service, National Bureau of Standards, Springfield, VA.

Eskilson, P. (1987) Thermal analysis of heat extraction boreholes, Doctoral Thesis, Lund University, Sweden.

Fortune, S. (1987) A sweepline algorithm for Voronoi diagrams. Algorithmica, 2, 153–174.

Freeman, C.M., Boyle, K.L., Reagan, M., Johnson, J., Rycroft, C., and Moridis, G.J. (2014) MeshVoro: A three-dimensional Voronoi mesh building tool for the TOUGH family of codes. Computers and Geosciences, 70, 26–34.

Fridleifsson, I.B. (2001) Geothermal energy for the benefit of the people, Renewable and Sustainable Energy Reviews, 5, 299-312.

Fujii, H., Itoi, R., and Ishikami, T. (2004) Improvements on analytical modeling for vertical U-tube ground heat exchangers, Geothermal Resources Council

Transactions, 28, 73-77.

Fujii, H., Itoi, R., Fujii, J., and Uchida Y. (2005) Optimizing the design of large-scale ground-coupled heat pump systems using groundwater and heat transport modeling, Geothermics, 34, 347–364.

Gehlin, S. (2002) Thermal response test: method development and evaluation, Doctoral Thesis, Luleå University of Technology, Sweden.

Gehlin, S. and Hellström, G. (2003) Influence on thermal response test by groundwater flow in vertical fractures in hard rock, Renewable Energy, 28, 2221-2238.

Green, P. and Sibson, R. (1978) Computing Dirichlet tessellations in the plane. The Computer Journal, 21, 168–173.

Haukwa, C. (1998) AMESH A mesh creating program for the integral finite difference method: A User's Manual. Lawrence Berkeley National Laboratory, Berkeley, California, 54 p.

Hellström, G. and Sanner, B. (2000) EED: Earth Energy Designer User manual, Version 2.0.

Incropera, F.P., DeWitt, D.P., Bergman, T.L., and Lavine, A.S. (2007) Introduction to heat transfer. Wiley, New York, 928 p.

Ingersoll, L.R. and Plass, H.J. (1948) Theory of the Ground Pipe Heat Source for the Heat Pump, Transactions of Amer. Soc. Of Heating and Ventilating Engineers, 54, 339-348.

Ingersoll, L.R., Adler, F.T., Plass, H.J., and Ingersoll, A.C. (1950) Theory of earth

heat exchangers for the heat pump, Transactions of Amer. Soc. Of Heating and Ventilating Engineers, 56, 167-188.

Karypsis, G. and Kumar V. (1998) METIS. A Software Package for Partitioning Unstructured Graphs, Partitioning Meshes, and Computing Fill-Reducing Orderings of Sparse Matrices, V4.0. Technical Report, Department of Computer Science, University of Minnesota.

Kavanaugh, S.P. (1984) Simulation and experimental verification of vertical ground-couple heat pump systems, Ph.D. Dissertation, Oklahoma State University, Stillwater, Oklahoma.

Kavanaugh, S.P. and Rafferty, K. (1997) Ground-Source Heat Pumps: Design of Geothermal Systems for Commercial and Institutional Buildings, American Society of Heating, Refrigerating and Air-Conditioning Engineers, Atlanta, GA.

Kim, S.K., Bae, G.O., Lee, K.K., Shim, B.O., and Song, Y. (2008) Model Development to Simulate Geothermal Heat Transport and Sensitivity Analyses on the Design Parameters of Closed-loop Geothermal Heat Pump System. Korean Society for Geosystem Engineering. 45 (4), 326-336.

Kim, S.K., Bae, G.O., Lee, K.K., and Song, Y. (2010) Field-scale evaluation of the design of borehole heat exchangers for the use of shallow geothermal energy. Energy, 35, 491–500.

Kohl, T., Hopkirk, R. J. (1995) "FRACTure" a simulation code for forced fluid flow and transport in fractured porous rock, Geothermics, 24, 345-359.

KS C 9306. (1999) Air Conditioners, Korean Agency for Technology and Standards.

Lund, J., Sanner, B., Rybach, L., Curtis, R., and Hellström, G. (2004) Geothermal (Ground-Source) Heat Pumps A World Overview. GHC BULLETIN, 25 (3), 1-10.

Message Passing Forum. (1994) A Message-Passing Interface Standard, International Journal of Supercomputing Applications and High performance Computing, 8, 3–4.

Morris, F.H. and Whitman, W.G. (1928). Heat Transfer for Oils and Water in Pipes1. Industrial and Engineering Chemistry, 20, 234–240.

Narasimhan, T.N. and Witherspoon, P.A. (1976) An Integrated Finite Difference Method for Analyzing Fluid Flow in Porous Media, Water Resour. Res., 12, 57-64.

Palagi, C.L. and Aziz, K. (1994) Use of Voronoi grid in reservoir simulation. Society of Petroleum Engineers Advanced Technology Series, 2, 69–77.

Pan, L. (2003) Wingridder - an interactive grid generator for TOUGH2. TOUGH Symposium 2003, Berkeley, California, May 12–14, p. 1–7.

Penrod, E.B. (1954) Sizing Earth Heat Pumps, Refrigerating Engineering, 62, 57-61.

Persson, P.O. and Strang, G. (2004) A simple mesh generator in MATLAB. Society for Industrial and Applied Mathematics review, 46, 329–345.

Pruess, K. (2004) The TOUGH codes - a family of simulation tools for multiphase flow and transport processes in permeable media. Vadose Zone Journal, 3, 738–746.

Pruess, K., and Narasimhan, T.N. (1982) On Fluid Reserves and the Production of Superheated Steam from Fractured, Vapor-Dominated Geothermal Reservoirs, J. Geophys. Res., 87, 9329 – 9339.

Pruess, K., and Narasimhan, T.N. (1985) A Practical Method for Modeling Fluid and Heat Flow in Fractured Porous Media. Soc. Pet. Eng. J., 25, 14-26.

Pruess, K., Oldenburg, C., and Moridis, G. (1999) TOUGH2 User''s Guide, V2.0, Lawrence Berkeley National Laboratory Report LBNL-43134, Berkeley, CA.

Rafferty, K. (2003) Ground Water Issues in Geothermal Heat Pump Systems, Ground Water, 41, 408-410.

Shim, B.O., Lee, Y., Kim, H.C., and Song, Y. (2006) Investigation of Thermal and Hydraulic Characteristics for the Performance Analysis of a Borehole Heat Exchanger, The Korean Society for Geosystem Engineering, 43 (2), 97-105.

Sieger, D., Alliez, P., and Botsch, M. (2010) Optimizing voronoi diagrams for polygonal finite element computations. In Proceedings of the 19th international meshing roundtable. Springer, Berlin, Heidelberg, p. 335–350.

Signorelli, S. (2004) Geoscientific investigations for the use of shallow low-enthalpy systems, for the degree of Doctor of Science, Swiss Federal Institute of Technology Zurich, Switzerland.

Signorelli, S., Bassetti, S., Pahud, D. and Kohl, T. (2006) Numerical evaluation of thermal response tests, Geothermics, 36, 141-166.

Spitler, J.D. (2000) GLHEPRO: A Design Tool For Commercial Building Ground Loop Heat Exchangers, Proceedings of the Fourth International Heat Pumps in

Cold Climates Conference, Aylmer, Quebec, August 17-18.

Tuminaro, R.S., Heroux, M., Hutchinson, S.A., and Shadid, J.N. (1999) Official Aztec user''s guide, Ver 2.1, Massively Parallel Computing Research Laboratory, Sandia National Laboratories, Albuquerque, NM.

Verma, S. and Aziz, K. (1996) Two-and three-dimensional flexible grids for reservoir simulation. In 5th European Conference on the Mathematics of Oil Recovery, Leoben, Austria, September 3–6, p. 143–156.

Voronoi, G. (1908) Nouvelles applications des paramètres continus à la théorie des formes quadratiques. Journal für die Reine und Angewandte Mathematik. 133, 97–178.

Warren, J.E. and Root, P.J. (1963) The Behavior of Naturally Fractured Reservoirs, Soc. Pet. Eng. J., Transactions, AIME, 228, 245-255.

Weatherill, N.P. (1988) A method for generating irregular computational grids in multiply connected planar domains. International Journal for Numerical Methods in Fluids, 8, 181–197.

Winterton, R.H.S. (1998) Where did the Dittus and Boelter equation come from? International Journal of Heat and Mass Transfer, 41, 809–810.

Xu, T., Sonnenthal, E., Spycher, N., and Pruess, K. (2004) TOUGHREACT User''s Guide: A Simulation Program for Nonisothermal Multiphase Reactive Geochemical Transport in Variably Saturated Geologic Media, Lawrence Berkeley National Laboratory Report LBNL-55460, Berkeley, CA.

Xu, T., Spycher, N., Sonnenthal, E., Zhang, G., Zheng, L., & Pruess, K. (2011)

TOUGHREACT Version 2.0: A simulator for subsurface reactive transport under non-isothermal multiphase flow conditions. Computers & Geosciences, 37, 763-774.

Yavuzturk, C., Spitler, J.D., and Rees, S.J. (1999) A Transient two-dimensional Finite Volume Model for the Simulation of Vertical U-Tube Ground Heat Exchangers, ASHRAE Transactions, 105(2).

Zhang, K., Wu, Y.S., and Pruess, K. (2008) User's Guide for TOUGH2-MP - A Massively Parallel Version of the TOUGH2 Code, Lawrence Berkeley National Laboratory Report LBNL-315E, Berkeley, CA.

# Abstract (in Korean)

밀폐형 지열히트펌프 시스템의 최적 설계 및 평가를 위해 세계적으로 널리 사용되는 지열-지하수 시뮬레이터 중 하나인 TOUGHREACT를 밀폐형 지열히트펌프 시스템의 시뮬레이션에 적합하게 수정하고 지중열교환기의 형태를 정밀하게 반영하는 그리드를 만들어주는 프로그램을 개발했다. 개발한 모델은 순환유체가 지중열교환기를 거치며 땅속에 열을 주입하거나 방출한 후 지상에서 다시 히트펌프와 열교환을 하는 일련의 과정을 특별한 가정 없이 완전한 3차원으로 계산할 수 있다. 한국지질자원연구원의 지진연구동에 설치된 밀폐형 지열히트펌프 시스템에서 수행된 열응답시험 및 실제 가동 자료를 모델 검증에 이용했고 시뮬레이션 결과와 아주 잘 일치했다. 검증을 마친 모델을 민감도 분석 및 시스템의 설계 평가에 적용했다. 시스템의 성능에 영향을 줄 수 있는 7개의 인자들에 대한 민감도 분석을 실시한 결과 땅의 열전도도가 가장 중요한 인자로 나타났다. 땅의 수리전도도가 $10^{-4}$ m/s 이상인 곳에서는 지하수의 흐름속도도 시스템의 성능에 큰 영향을 준다. 한국지질자원연구원에 설치된 28개의 지중열교환기와 79개의 히트펌프에 대해 시스템의 설치에 들어간 초기 비용과 시스템을

2030년까지 가동할 때 필요한 가동 비용을 시뮬레이션을 통해 분석하여 설계가 잘 이루어졌는지 평가했다. 전기세의 변화를 현재의 물가상승률을 고려하여 예측했을 때 두 비용의 합이 가장 작은 경우는 총 지중열교환기의 수가 16개인 경우로 나타났다. 현재 설치된 지중열교환기가 가장 비용효율적이 되는 경우는 전기세가 4배 정도 더 비쌀 때로 나타났다. 처음 개발된 모델은 지중열교환기를 1개 밖에 고려하지 못하기 때문에 다수의 지중열교환기를 고려하기 위해 병렬계산이 가능한 TOUGH2-MP를 TOUGHREACT에서 한 것과 마찬가지로 수정했고 그리드 생성 프로그램도 그에 맞게 개선되었다. 다수의 지중열교환기를 한번에 계산할 경우 시스템 가동 시 지중열교환기 사이의 열적 간섭 현상과 가동이 끝난 후 변화된 땅속의 온도가 다음 계절의 가동에 미치는 영향을 고려할 수 있다. 병렬계산은 그리드의 수가 대폭 증가되므로 계산 시간을 줄이고 메모리를 확보하기 위해 도입되었다. 속도테스트 결과 프로세서 수의 증가에 따른 속도향상이 거의 정비례했다. 개발된 모델을 한국지질자원연구원의 지열히트펌프 시스템의 장기 가동 시 성능 평가에 적용했다. 가상의 가동 패턴을 설정하여 25년간 성능 평가를 실시한 결과 냉방시즌에 땅으로 방출되는 열량이 난방시즌에 땅에서 흡수되는 열량보다 커서

지중열교환기 주변의 지온이 점점 상승하고 냉방시즌의 시스템 성능이 지속적으로 감소하는 것으로 나타났다. 실제 지하수 온도 모니터링 자료에서도 비슷한 현상이 관측되었으므로 좀 더 장기적인 모니터링 후 온도 증가가 지속된다면 가동 패턴에 변화를 줄 필요가 있다. 마지막으로 밀폐형 지열히트펌프 시스템뿐만 아니라 개방형 및 standing column well 지열히트펌프 시스템도 고려할 수 있도록 모델을 개선했다. 특히 그리드를 Voronoi 다이어그램 형태로 만들어서 관정이나 파이프의 형태를 자유롭고 정밀하게 나타낼 수 있게 되었고 TOUGH2 계열의 프로그램에서 사용되는 integrated finite difference 방법에서 인접한 그리드블록의 중점을 연결한 선과 두 그리드블록의 경계선이 직교해야 하는 조건도 항상 만족시킬 수 있게 되었다. 개발된 모델은 간단한 테스트 과정만 거쳤고 검증 및 적용은 추후 연구를 통해 진행할 예정이다.

**주요어**: 지열히트펌프, 지중열교환기, 최적설계, 장기성능예측, TOUGH2, integral finite difference method

**학번**: 2004-20564